JOURNAL OF PETROLOGY | VOLUME 38 | NUMBER 6 | PAGES 785–813 | 1997

The Petrogenetic Evolution of Lavas from Easter Island and Neighbouring Seamounts, Near-ridge Hotspot Volcanoes in the SE Pacific

KARSTEN M. HAASE[1,2]*, PETER STOFFERS[1] AND C. DIETER GARBE-SCHÖNBERG[1]

[1]GEOLOGISCH-PALÄONTOLOGISCHES INSTITUT DER UNIVERSITÄT KIEL, OLSHAUSENSTR. 40, 24118 KIEL, GERMANY

[2]MAX-PLANCK-INSTITUT FÜR CHEMIE, POSTFACH 3060, 55020 MAINZ, GERMANY

RECEIVED ON JUNE 20, 1996 REVISED TYPESCRIPT ACCEPTED FEBRUARY 10, 1997

Major and trace element, mineralogical and petrographical data are presented for submarine and subaerial lavas from Easter Island and two neighbouring seamounts. The samples can be divided into three groups based on their major element composition and incompatible element enrichment, typified by their $(La/Sm)_N$ ratios. Tholeiitic samples with $(La/Sm)_N$ of ~1·2 are comparable with lavas constituting three young volcanic fields closer to the spreading axis. The other two lava series from Easter Island and the two seamounts are transitional to slightly alkaline, one having an intermediate enrichment with $(La/Sm)_N$ of 1·5–2, the other being even more enriched [$(La/Sm)_N$ ~2·3]. Large phenocrysts and xenocrysts of olivine and plagioclase in the submarine lavas indicate a crustal reservoir with crystallizing magma. Compared with the relatively mafic submarine samples, the more fractionated lavas on Easter Island suggest the presence of another, more shallow magma chamber. The extreme differentiation of rhyolites and trachytes probably occurred as a result of decreasing magma supply during waning phases of volcano activity. Each volcano of the Easter Hotspot probably evolved through at least two stages. A tholeiitic stage appears to form large volcanoes at depths >1000 m and is succeeded by a transitional group of lavas which can be observed on Easter Island. A third stage with the most enriched lavas may form small eruptive centres on the flanks of older volcanoes or as flank cones on the seafloor. The degree of partial melting decreases from the tholeiitic to the most enriched alkaline series. The occurrence of different stages of volcanism at the Easter Hotspot not only resembles the magmatism of other Pacific hotspots such as Hawaii but also the volcanism of non-plume near-ridge seamounts at the East Pacific Rise. We suggest that the development of each magmatic stage depends on the age of the overlying plate, which determines (1) the amount of depleted mid-ocean ridge material mixed into the magma source and (2) the degree of partial melting.

KEY WORDS: *Easter Island; fractional crystallization; magmatic evolution; oceanic magmatism; partial melting*

INTRODUCTION

Intraplate volcanoes are widespread on Earth and make up large parts of the oceanic crust in many regions such as the East Pacific (Abers *et al.*, 1988). Oceanic islands and seamounts have received much attention because their chemistry is not directly affected by contributions from continental material and thus they are relatively simple magmatic systems compared with continental volcanoes. Nevertheless, many oceanic intraplate volcanoes display a wide range of chemical compositions varying during the lifetime of the magmatic system. These compositional changes can be attributed both to melting

*Corresponding author. Present address: Lamont–Doherty Earth Observatory of Columbia University, Palisades, NY 10964, USA. Telephone: 1 914 365 8907. Fax: 1 914 365 8155. e-mail: karsten@ldgo.columbia.edu

processes in the mantle as well as to shallow-level differentiation. Because the oceanic crust probably does not significantly contaminate the oceanic magmas, both the partial melting and the crystal fractionation processes responsible for generating the compositional variability of the erupted lavas can be modelled with greater ease than for continental volcanoes. Large intraplate volcanoes built on thick lithosphere, such as Hawaii, develop through several stages of volcanism, probably depending on the spatial relationship of the volcano to its magma source in a mantle plume (e.g. Chen & Frey, 1985). It appears that the degree of partial melting, the source of the magmas and their crystal fractionation history change with time at Hawaii (e.g. Clague & Dalrymple, 1987). A temporal change in the chemistry of the erupting magmas has also been shown to exist for near-ridge seamounts (Batiza & Vanko, 1984; Zindler *et al.*, 1984). Variations in the chemical composition of primitive magmas of oceanic intraplate volcanoes have been attributed to the age of the underlying crust (McBirney & Gass, 1967; Baker, 1973; Haase, 1996). This relationship is probably due to an increase in the depth of the zone of partial melting as the lithosphere thickens with age, irrespective of whether the volcanoes are of plume (Ellam, 1992) or non-plume origin (Batiza, 1980). The differentiation of primary oceanic intraplate magmas can lead to some extremely silica-rich lavas such as rhyolites and trachytes, and the study of these processes gives insight into an important chemical fractionation process on Earth which possibly also generated parts of the continental crust (O'Nions & McKenzie, 1988). Thus, the investigation of the petrogenesis of oceanic intraplate magmatism can help to constrain magmatic processes in different plate tectonic settings.

The abundant young volcanism between Easter Island and the East Rift spreading axis of the Easter Microplate in the Southeast Pacific provides an opportunity to study magmatic processes close to a spreading centre, away from which the lithosphere thickens quickly with increasing age. In this paper, we present major and trace element and mineralogical data for the intraplate volcanics of Easter Island and two neighbouring seamounts. A petrogenetic model is developed in which we define three different magma groups, each of which probably has its own liquid line of descent. The three magma groups originate by different degrees of partial melting of mantle sources containing varying amounts of mid-ocean ridge basalt (MORB) source mantle material mixed with an enriched plume component. Each magma type is generated in a different environment depending on the thickness (age) of the overlying lithosphere and the distance from the spreading axis (input of MORB source material).

GEOLOGICAL SETTING

Easter Island lies ~3500 km to the west of the South American coast and 350 km east of the Easter microplate (Fig. 1). The Easter microplate formed ~5 Ma ago when the eastern spreading segment of the East Pacific Rise propagated northwards forming a large overlap with the western ridge axis (Naar & Hey, 1991). As a result of this propagation the crust of the microplate was rotated. Easter Island lies close to the eastern pseudofault of the propagator (Naar & Hey, 1991; Searle *et al.*, 1993). The 2500 km long and 100 km wide Easter Seamount Chain (ESC), or Sala y Gomez Ridge, stretches to the east of the island. The ESC is bounded to the east by the Nazca Ridge, a 300 km wide aseismic ridge extending to South America (Woods & Okal, 1994). The ESC shows an age progression, with the youngest volcanoes occurring in the west near Easter Island (O'Connor *et al.*, 1995). Between Easter Island and the East Rift spreading axis of the Easter microplate a large area of young volcanism was discovered during recent US and German cruises (Hagen *et al.*, 1990; Stoffers *et al.*, 1994). Two large seamounts, Moai and Pukao, rise to only a few hundred metres below sea-level (Fig. 1). Closest to the spreading axis and ~150 km west of Easter Island, three volcanic fields were found and named Ahu, Umu and Tupa. These volcanic fields consist mainly of incompatible element enriched tholeiitic lavas originating from a mantle source that resulted from mixing of depleted MORB source material with an enriched source material in the Easter plume (Haase & Devey, 1996; Fretzdorff *et al.*, 1996; Haase *et al.*, 1996).

Easter Island has a roughly triangular shape with the three volcanoes Poike, Rano Kau and Terevaka on each corner (Fig. 1b). Its surface area is ~160 km^2 and it rises to 510 m above sea-level. A 50 km long submarine ridge, the Rano Kau Ridge, extends from Rano Kau volcano towards the southwest (Hagen *et al.*, 1990). The age relationships of the Easter Island volcanism are relatively well known from stratigraphy and radiometric dating. Although some of the early work suggested ages of 3–1·89 Ma for lavas at the base of the oldest volcano, Poike (Baker *et al.*, 1974; Clark & Dymond, 1977), a more recent investigation of these flows gave reproducible ages of $0{\cdot}52 \pm 0{\cdot}29$ Ma and $0{\cdot}69 \pm 0{\cdot}15$ Ma (Kaneoka & Katsui, 1985). The younger ages are in accordance with most age determinations of Easter Island lavas, which are <0·7 Ma for all three volcanoes (Gonzalez-Ferran *et al.*, 1974; Clark & Dymond, 1977; Kaneoka & Katsui, 1985; O'Connor *et al.*, 1995). Kaneoka & Katsui (1985) attributed the scatter observed in the K–Ar ages of Clark & Dymond (1977) to atmospheric Ar contamination. The strongly eroded volcanoes Poike and Rano Kau are older than the third volcano, Terevaka, and their activity apparently ended with the emplacement of trachytic and

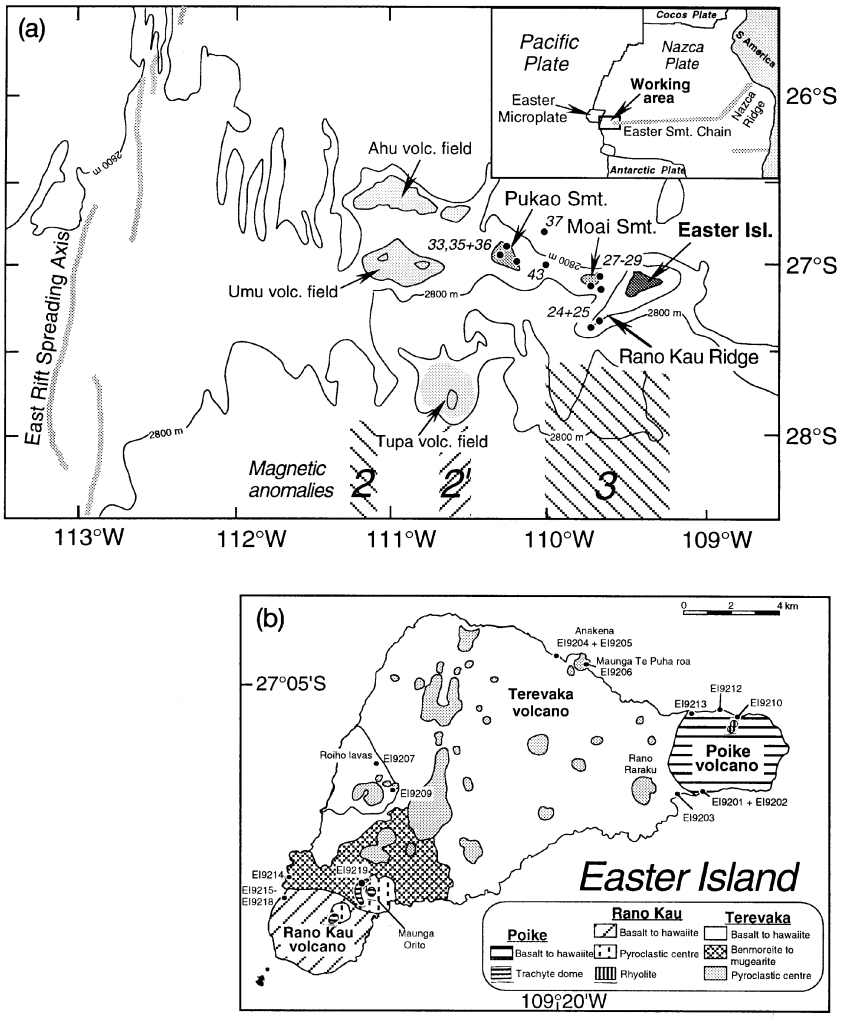

Fig. 1. (a) Location map of Easter Island and the seamounts Moai and Pukao redrawn after Naar & Hey (1991). The dots mark the dredge sites on the submarine volcanoes and the inset the location of the working area in the SE Pacific. The diagonal patterns indicate the approximate locations of the magnetic anomalies 2, 2′ and 3 as determined by Naar & Hey (1991), which correspond to ages of ~1·5–4 Ma (Harland *et al.*, 1990). (b) Geological map of Easter Island redrawn after Baker *et al.* (1974), showing the sample localities.

rhyolitic intrusions at Poike and Rano Kau, respectively (Fig. 1b). The late intrusions of Rano Kau have been dated at $0{\cdot}24 \pm 0{\cdot}04$ Ma by Kaneoka & Katsui (1985) and $0{\cdot}34 \pm 0{\cdot}06$ and $0{\cdot}18 \pm 0{\cdot}03$ Ma by Gonzalez-Ferran *et al.* (1974). Palaeomagnetic surveys indicate that lavas from all three volcanoes on Easter Island erupted in times of normal polarity (Isaacson & Heinrichs, 1976; Kaneoka & Katsui, 1985), i.e. probably in the Brunhes normal epoch, which began 0·75 Ma ago (Harland *et al.*, 1990). The lavas of Terevaka volcano have ages <0·4 Ma, which is also the estimated age of most of the submarine volcanism west of Easter Island based on the high reflectivity observed on side-scan sonar maps (Hagen *et al.*, 1990). The Roiho lava field lies on the flank of the young Terevaka volcano, and is stratigraphically young, having only a thin vegetation cover. O'Connor *et al.* (1995) have recently dated the Roiho field lavas at $0{\cdot}13 \pm 0{\cdot}02$ Ma, which is younger than the age those researchers determined for two samples from Moai and Pukao seamounts further west of Easter Island ($0{\cdot}63 \pm 0{\cdot}18$ Ma and $0{\cdot}23 \pm 0{\cdot}08$ Ma, respectively). One lava from the Umu volcanic field yielded an Ar–Ar plateau age of $2{\cdot}5 \pm 0{\cdot}5$ Ma (isochron age $3{\cdot}0 \pm 1{\cdot}1$ Ma, O'Connor *et al.*, 1995) but this age is not well constrained because it was calculated using only 48% of the ^{39}Ar and comes from a sample with low K_2O content (0·1–0·2%, Fretzdorff *et al.*, 1996). We suggest that the young age of the volcanism of the Easter Hotspot (<0·7 Ma) indicates that all the magmas formed in an intraplate region because the age of the underlying plate ranges from ~4 Ma beneath Easter Island to less than ~2 Ma beneath the volcanic fields 200 km further west (magnetic

anomalies 2–3; Naar & Hey, 1991). Thus, the Easter microplate apparently formed considerably earlier than the Easter Island volcanoes.

The shallow bathymetry around Easter Island, its location at the young end of a volcanic chain, the volume of young volcanics, and their enriched geochemistry suggest that there is a mantle plume underneath the area (Hagen *et al.*, 1990; Haase *et al.*, 1996). Other models which have been proposed for the origin of the Easter Hotspot and the ESC are a mantle hotline (Bonatti *et al.*, 1977), a propagating fracture (Clark & Dymond, 1977), an incipient oceanic rift (Mammerickx, 1981), or the location of Easter Island above a plume-channel from a plume further east near Sala y Gomez (Schilling *et al.*, 1985; O'Connor *et al.*, 1995).

SAMPLING AND METHODS

The area was sampled during the SO80 cruise of FS *Sonne* in June–July 1992, and during a stay of 1 week on Easter Island after the cruise. The submarine samples were recovered by dredging, and the dredge sites are shown in Fig. 1 and in Table 1. From each dredge, samples were chosen based on macroscopic petrographic features (e.g. phenocryst content, vesicularity) and analysed for major elements. Samples showing a range of different chemical compositions were selected for trace element and Sr, Nd and Pb isotope analysis (Haase, 1995; Haase *et al.*, 1996). Three dredges were taken on Moai seamount (Table 1, Fig. 1), recovering slightly altered lavas with fresh glass rims. Another three dredges were taken on the top of Pukao seamount and one on a large flank cone north of the main edifice (Fig. 1). The dredge on the side cone (37DS) recovered the freshest material from Pukao seamount with abundant glass crusts. The lavas recovered from the submarine part of Easter Island (the Rano Kau Ridge) and those from the two seamounts consist mainly of pillow lavas with rare sheet flow fragments. Glass crusts occurred on most samples and the glass was generally fresh without palagonitization.

The subaerial samples were collected based on descriptions of the geology of the island (Gonzalez-Ferran *et al.*, 1968, 1974; Baker *et al.*, 1974) and selected for their freshness. We tried to collect only fresh samples from the island (for example, at sea cliffs and road cuts). These samples were sawn, and from samples with abundant glass we separated glass for geochemical analysis, whereas for the samples without glass the analysis was perfomed on pillow interiors sawn from massive pieces. After removal of all visible signs of alteration, the lava pieces were washed in an ultrasonic bath. Then the samples were crushed and rinsed several times in distilled water in an ultrasonic bath. The samples were then powdered in an agate mill. The procedure for glass was similar except that, after the crushing, clean glass was hand-picked for all analyses.

Major elements were analysed on fused glass discs with a Philips 1400 X-ray fluorescence (XRF) machine using international rock standards for calibration. Loss on ignition (LOI) was not determined because the Fe^{2+}/Fe^{3+} ratios of the samples are unknown and the oxidation of the ferrous iron adds a significant uncertainty to the LOI determination. The results for the international standard BHVO-1 measured as an unknown are given in Table 6 (below). With the exceptions of Na_2O and P_2O_5, the results show a precision and accuracy better than 1%. Some glasses and mineral phases were analysed with a Cameca CAMEBAX electron microprobe of the Mineralogical Institute in Kiel. Trace elements were measured with the Plasmaquad PQ1 inductively coupled plasma mass spectrometer at the Geological Institute in Kiel after the method described by Garbe-Schönberg (1993). The average of ten measurements of the rock standard BHVO-1 analysed with the samples and the standard deviations are presented in Table 7 (below). The precision and accuracy for most elements are better than 5%. To lower the problems with isobaric interference, the highly enriched samples such as EI9219 were measured at a higher dilution factor than that given by Garbe-Schönberg (1993).

RESULTS

Petrography and mineral chemistry

With the exception of the glassy rhyolites and some pyroclastic rocks, all lavas from Easter Island are holocrystalline whereas the submarine samples have thick glassy rims. The most abundant phenocryst phase in the Easter Island samples is plagioclase, which is accumulative in some basalts (Table 1a), whereas olivine and clinopyroxene occur only rarely as phenocrysts in the lavas. This is in contrast to the Moai seamount lavas, where the dominating phenocryst phases are olivine and plagioclase, whereas clinopyroxene occurs only in subordinate amounts as microphenocrysts (Table 1b). All samples from Moai seamount are petrographically similar with slight variations in the volumes of phenocrysts, whereas the Pukao seamount volcanics are variable, with plagioclase-cumulative (35DS-1 to -4) to aphyric samples and volcanic breccias. The less phyric Pukao lavas generally resemble the Moai samples in terms of petrography. The older-looking 24DS samples from the Rano Kau Ridge are plagioclase cumulates, whereas the very fresh 25DS samples are only slightly porphyritic and contain few phenocrysts of plagioclase and olivine in a glassy matrix. The matrix of most submarine samples contains glass and skeletal crystals, in contrast to the holocrystalline

Table 1: (a) Petrography of the Easter Island samples; the modal abundance of minerals was estimated from thin sections and is given in vol. %

Sample	Location	Petrography
EI9201	SE foot of Poike	Ph: ~3% ph of plag and ~2% cpx (<1 mm), 5% ves
		Matrix: of plag laths and intergranular cpx + Ti-mt
EI9202	SE foot of Poike, flow above EI9201	Ph: 5% plag (<2 mm), few cpx (<1 mm)
		Matrix: plag laths and intergran. cpx + Ti-mt
EI9203	Hotu Iti	Ph: 10% ol (<1 mm) + plag (<5 mm), 5% ves
		Matrix: plag laths, intergran. cpx + Ti-mt + ol
EI9204	Anakena, Terevaka volcano	Ph: 10% plag (–10 mm) and 5% cpx (–5 mm), cumulate xenos with plag, cpx and ol, 10% ves
		Matrix: plag laths with intergranular cpx and Ti-mt
EI9205	Anakena, Terevaka volcano	Ph: plag (<20 mm) + ol (<1 mm), 25% ves
		Matrix: plag laths + intergran cpx + Ti-mt
EI9206	Maunga Te Puha, Ovahe	~2% mph plag + cpx, 20% ves
		Matrix: plag laths in tachylitic groundmass
EI9207	Roiho lava field	Ph: 5% ol (<1 mm), 15% ves
		Matrix: plag laths + intergran cpx + ol +Ti-mt
EI9209	Roiho lava field	Aphyric, 40% vesicles, seriate-textured ol + plag (<1 mm), intergran cpx + Ti-mt
EI9210	Maunga Parehe	Ph: 7% anorthoclase (<2 mm), 3% cpx, 5% ves.
		Matrix: alk fsp + aeg–aug + Ti-mt
EI9212	Top of cliff, NW Poike	Ph: 30% plag (<10 mm) + few ol (<1 mm), 20% ves
		Matrix: plag laths + intergran cpx + ol + Ti-mt
EI9213	NW Poike	Ph: 17% plag (<5 mm) + 3% ol (<0·5 mm), 10% ves
		Matrix: plag laths (<0·5 mm) + intergran cpx + Ti-mt
EI9214	Ana Kai Tangata	Ph: 2% plag (<2 mm), 15% ves
		Matrix: plag + cpx (<0·5 mm) + Ti-mt+ ilm
EI9215	Lowest flow, SE cliff of Rano Kau	Ph: 5% plag (<2 mm) + few cpx, 40% ves
		Matrix: plag laths + intergran cpx + ol + Ti-mt
EI9216	Flow above EI 9215	Ph: 5% plag (<1 mm), 10% ves
		Matrix: plag laths + intergran cpx + Ti-mt
EI9217	Flow above EI9216	Ph: 10% plag (<1 mm), ol mph (<0·1 mm), 25% ves
		Matrix: plag laths + intergran cpx + ol + Ti-mt
EI9218	Flow above EI9217	Ph: 2% plag (<1 mm), 10% elongated ves
		Matrix: plag laths + cpx + ol + Ti-mt
EI9219	Maunga Orito	Tiny crystals (<0·2 mm) of anorthoclase and fayalite in colourless glass

Plag, plagioclase; ol, olivine; cpx, clinopyroxene; Ti-mt, titanomagnetite; alk fsp, alkali feldspar; ilm, ilmenite; ves, vesicles; ph, phenocrysts; mph, microphenocrysts; intergran, intergranular.

matrix of the subaerial lavas (Table 1b). Vesicles in the rocks from dredge 33DS are filled with calcite and zeolites, although the olivines are generally unaltered, indicating some hydrothermal alteration of the samples.

The composition of the feldspars in Easter Island rocks ranges from plagioclase with An_{69} in the basalt EI9203 to anorthoclase in the trachyte EI9210 (Fig. 2 and Table 2). All phenocrysts are higher in An than the matrix feldspars. Olivine occurs in many volcanic rocks on Easter Island as a phenocryst phase, and shows a very large compositional range from Fo_{77} in basaltic lavas to Fo_1 in trachytes (Fig. 3 and Table 3). Relative to the large range of feldspar and olivine compositions observed in the Easter Island lavas, the seamounts display limited compositional ranges. The olivine compositions in the investigated samples from Moai and Pukao range from Fo_{83} to Fo_{79}, and the An content of the plagioclase is ~71; both minerals usually display a strong normal zonation (Figs 2 and 3, Tables 2 and 3). The plagioclase and olivine phenocrysts of the submarine samples have

Table 1: (b) Locations of the dredge sites and petrographical descriptions of representative samples from the submarine volcanoes of the Easter Hotspot

Sample no.	Dredge start and end	Water depth (m)	Petrography
24DS-2, Rano Kau Ridge	27°22·03′S, 109°34·22′W to 27°21·91′S, 109°34·64′W	2294–2053	Ph: ~40 plag (–10 mm), few ol ph (–3 mm); Matrix variolitic, ~10% vesicles
25DS-1, Rano Kau Ridge	27°23·38′S, 109°40·27′W to 27°22·61′S, 109°40·97′W	2144–1506	Ph: ~2% plag (–0·5 mm) and ~1% ol (–1 mm); Matrix intersertal glass, ~20% vesicles
25DS-2			Ph: ~1% plag (–0·4 mm) and 3% ol (–0·5 mm); Matrix cpx + tachylite; ~5% vesicles
26DS-1, Moai Seamount	27°10·00′S, 109°39·91′W to 27°08·21′S, 109°39·78′W	1727–1355	Ph: ~5% plag (–5 mm), ~4% cpx (–1 mm) and ~1% ol (–1 mm); Matrix: intergranular cpx + opaques, 10% vesicles
26 DS-2			Ph: ~30% plag (–3 mm), ~10% cpx (–0·5 mm), ~5% ol (–1 mm); Matrix: plag laths intergranular cpx + opaques; 20% vesicles
27DS-1, Moai Seamount	27°04·42′S, 109°36·64′W to 27°04·81′S, 109°36·31′W	1896–1781	Ph: ~3% ol (–1 mm), ~2% plag (–1 mm); Matrix variolitic plag + ol in tachylitic glass, 20% vesicles
27DS-2			Ph: ~5% plag (–1 mm), 5% ol (–1 mm); Matrix skeletal plag, cpx and opaques; 10% vesicles
28DS-2, Moai Seamount	27°07·49′S, 109°39·45′W to 27°07·08′S, 109°39·47′W	1214–964	Ph: ~5% plag (–1 mm), 5% ol (–0·5 mm); Matrix altered glass + microlites; ~20% vesicles
29DS-1, Moai Seamount	27°07·48′S, 109°39·49′W to 27°06·93′S, 109°39·62′W	1284–1068	Seriate textured basalt, ol (–1 mm), plag (–1 mm); Matrix tachylitic; ~30% vesicles
29DS-2			Ph: ~15% plag (–4 mm), 10% ol (–2 mm), ~3% cpx (–1 mm); Matrix: tachylitic glass, 30% vesicles
29DS-3			Ph: ~15% plag (–4 mm), 15% ol (–2 mm), 5% cpx (–1 mm); Matrix: skeletal cpx, plag and opaques; 30% vesicles
33DS-1, Pukao Seamount	26°55·69′S, 110°17·81 W to 26°55·66′S, 110°17·70′W	523–408	Ph: ~15% plag (–5 mm), ~3% ol (–0·5 mm), ~2% cpx (–0·5 mm), filled Matrix: plag, cpx, ol, opaques and intersertal glass; ~20% vesicles with zeolites and carbonate
35DS-1a, Pukao Seamount	26°55·45′S, 110°18·41′W to 26°55·90′S, 110°18·26′W	989	Ph: ~30% plag (–10 mm), 5% ol (–3 mm), 5% cpx (–3 mm); Matrix: plag laths + intergranular cpx, ol and opaques; no vesicles
35DS-4			Hyaloclastite consisting of three different rock types
35DS-10			Ph: ~2% plag (–1 mm); Matrix: grains of plag, ol, cpx with interstitial altered glass,~2% vesicles
36DS-1, Pukao Seamount	26°58·25′S, 110°13·37′W to 26°58·51′S, 110°13·99′W	1027–751	Ph: ~20% ol (–2 mm), ~10% plag (–1 mm), Matrix: plag laths + intergranular cpx +opaques, ~30% vesicles
36DS-4			Ph: ~10% ol (–2 mm), ~10% plag (–1 mm); Matrix microlites and glass; ~40% vesicles
37DS-1, cone N of Pukao Smt.	26°50·02′S, 110°02·96′W to 26°49·52′S, 110°03·44′W	2890–2840	Ph: ~2% plag, ~1% ol, Matrix: skeletal plag and ol; microlites and glass; 20% vesicles
43DS-1, cone betw. Pukao and Moai	27°02·95′S, 110°02·72′W to 27°02·32′S, 110°02·78′W	2013–1698	Ph: ~3% ol (–1 mm), ~2% plag (–2 mm), Matrix: plag laths + intergranular cpx + ol, 10% vesicles
43DS-2			Ph; ~3% ol (–1 mm), glomerophyric, Matrix: microlites and glass, ~20% vesicles

more primitive compositions than the phases in the subaerial lavas. However, the most primitive olivine and plagioclase crystals were observed in the Rano Kau Ridge sample 24DS-2, which contains olivine and plagioclase with Fo_{85} and An_{78}, respectively (Tables 2 and 3). This plagioclase cumulative rock contains large strongly zoned and An-rich plagioclase crystals, whereas the phenocrysts have $An_{71–73}$ (Fig. 2). Sample 24DS-2 also contains large normally zoned olivines with Fo_{85} which are distinct from the significantly smaller phenocrysts with Fo_{82} (Table 3). Thus, the large crystals with primitive compositions are probably xenocrysts picked up by the magma on its way

Table 2: Compositions of representative feldspar crystals in Easter Hotspot samples

Sample:	24DS-2	24DS-2	24DS-2	36DS-4	36DS-4	36DS-4	EI9204 xenolith	EI9204 xenolith	EI9204	EI9204	EI9204	EI9203	EI9203	EI9210	EI9210	EI9210
Crystal:	Xeno	Xeno	M'pheno	Pheno	Pheno	M'pheno	Xeno	Xeno	Pheno	Pheno	Matrix	Pheno	Pheno	Pheno	Pheno	Matrix
Location:	Centre	Rim	Centre	Centre	Rim	Rim	Centre	Rim	Centre	Rim		Centre	Rim	Centre	Rim	
SiO_2	49·88	49·94	52·23	51·57	51·52	51·52	51·27	50·56	50·70	52·49	55·08	50·92	53·31	66·04	66·12	67·43
Al_2O_3	31·35	31·47	29·20	29·80	30·03	30·12	29·96	30·62	30·16	28·91	26·97	30·71	28·92	20·82	20·43	18·61
FeO	0·38	0·55	0·78	0·52	0·61	0·62	0·68	0·67	0·60	0·66	0·94	0·62	0·66	0·18	0·16	0·86
MgO	0·20	0·26	0·37	0·20	0·18	0·18	0·12	0·07	0·10	0·14	0·07	0·12	0·15			
CaO	15·95	15·97	16·9	14·47	14·48	14·45	14·56	15·22	14·75	13·45	10·57	14·77	12·94	1·90	1·67	0·18
Na_2O	2·43	2·41	3·39	3·20	3·12	3·09	3·67	3·28	3·43	4·23	5·59	3·65	4·63	9·06	8·71	7·52
K_2O	0·05	0·05	0·09	0·09	0·11	0·09	0·11	0·12	0·10	0·21	0·42	0·10	0·16	1·91	2·26	5·35
Total	100·27	100·74	100·11	99·99	100·24	100·20	100·37	100·54	99·86	100·09	99·64	100·89	100·77	99·91	99·45	100·04
An	78·2	78·4	73·1	71·1	71·5	71·8	68·3	71·5	70·0	63·0	50·0	68·8	60·2	9·3	8·3	0·9
Ab	21·5	21·4	26·5	28·4	27·8	27·7	31·1	27·8	29·4	35·8	47·7	30·7	38·9	79·9	78·5	67·9
Or	0·3	0·03	0·5	0·5	0·06	0·5	0·6	0·7	0·6	1·1	2·3	0·5	0·09	10·9	13·1	31·2

Table 3: Electron microprobe analyses of representative olivine crystals in the Easter Hotspot lavas

Sample:	36DS-4	36DS-4	24DS-2	24DS-2	29DS-2	EI9204	EI9203	EI9203	EI9203	EI9203	EI9203	EI9203	EI9203	EI9212	EI9212	EI9210
Crystal:	Pheno	Pheno	Pheno	Xeno	Pheno	Xeno	Pheno	Pheno1	Pheno1	Matrix1	Matrix2	Matrix3	Matrix	Pheno	Matrix	Pheno
Location:	Centre	Rim	Centre	Centre	Rim	Centre	Rim	Centre	Rim					Centre		Centre
SiO_2	40·03	39·937	41·68	40·34	39·34	37·97	35·51	35·51	35·20	33·44	33·40	33·20	33·44	38·73	34·13	29·73
FeO	15·59	17·49	14·13	13·95	18·95	26·15	37·62	37·62	41·32	47·74	48·10	51·07	48·44	21·25	41·54	65·89
MnO	0·27	0·30	0·16	0·20	0·36	0·46	0·59	0·59	0·61	0·72	0·79	0·73	0·85	0·33	0·61	2·46
MgO	44·51	41·36	41·57	46·15	41·00	36·23	26·34	26·34	22·80	17·88	17·22	14·63	16·48	39·78	22·71	0·44
CaO	0·25	0·53	1·27	0·30	0·36	0·28	0·33	0·33	0·40	0·54	0·45	0·48	0·47	0·31	0·38	0·63
Total	100·66	99·61	98·81	100·94	100·00	101·09	100·39	100·39	100·44	100·47	100·17	100·35	99·68	100·40	99·36	99·15
Fo cont.	83·3	80·2	82·5	85·2	79·0	70·9	55·2	55·2	49·3	39·7	38·7	33·5	37·4	76·6	49·0	1·2

Table 4: Electron microprobe analyses of representative clinopyroxene crystals in the Easter Hotspot lavas

Sample:	EI9204	EI9204	EI9204	EI9204	EI9204	EI9203	EI9203	EI9212	29DS-2	29DS-2	29DS-2
Crystal:	Xeno	Xeno	Pheno	Pheno	Matrix	M—pheno	Matrix	Matrix	Pheno	Pheno	Matrix
Location:	Centre	Rim	Centre	Rim					Centre	Rim	
SiO_2	50·46	50·91	51·41	50·47	50·88	50·07	51·56	47·41	50·46	48·88	43·80
TiO_2	1·40	1·29	1·08	1·48	1·39	1·39	1·03	3·19	1·35	1·93	4·53
Al_2O_3	3·49	3·27	2·44	2·94	1·77	2·47	1·14	3·81	4·51	5·71	7·75
FeO	7·48	7·67	8·40	8·80	12·78	13·14	15·66	12·00	6·16	6·68	12·48
MnO	0·15	0·21	0·22	0·20	0·35	0·31	0·36	0·24	0·10	0·11	0·23
MgO	14·71	14·85	14·62	14·42	13·68	12·35	12·41	12·44	15·72	14·81	9·48
CaO	21·51	21·08	20·66	20·54	18·42	19·70	18·06	20·18	21·46	21·39	20·99
Na_2O	0·43	0·42	0·40	0·50	0·41	0·49	0·47	0·44	0·35	0·35	0·57
Total	100·27	100·29	100·06	99·83	100·07	100·24	100·79	99·75	100·11	100·83	99·83
Wo	45·0	44·2	43·4	43·3	38·8	41·8	38·0	43·1	44·6	45·3	47·8
En	42·8	43·3	42·8	42·3	40·1	36·5	36·3	36·9	45·4	43·7	30·0
Fs	12·2	12·6	13·8	14·5	21·0	21·8	25·7	20·0	10·0	11·1	22·2

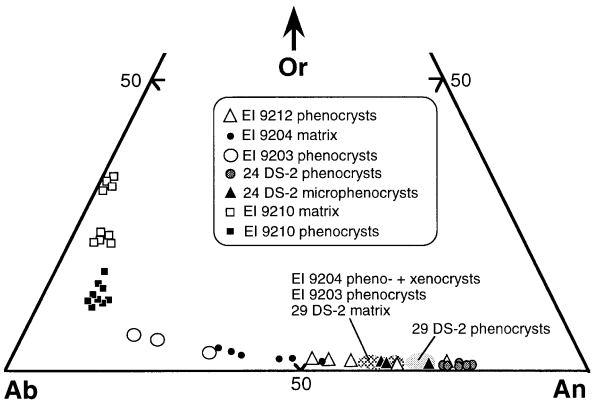

Fig. 2. Part of the Or–Ab–An triangle showing the feldspar compositions of samples from the Easter Hotspot.

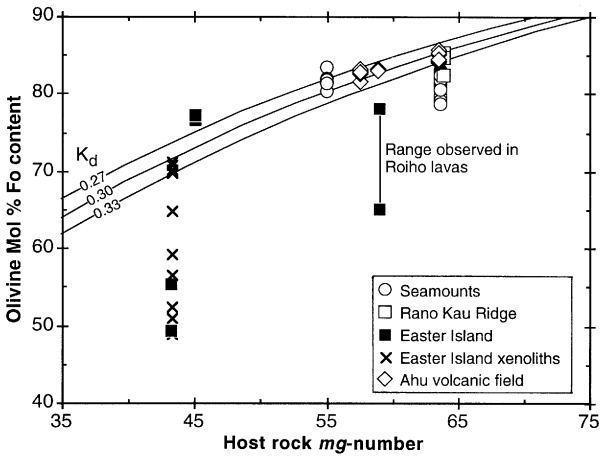

Fig. 3. Diagram of olivine phenocryst compositions plotted vs the *mg*-number of their host lava (whole rock or glass). For comparison we show the olivine compositions of the volcanic field tholeiites (Haase & Devey, 1996). The most primitive Easter Island lava and the olivine compositions are from Baker *et al.* (1974). The curves represent compositions with $K_d^{Ol\text{-}Liq}$ of 0·27, 0·30 and 0·33 where olivine is in equilibrium with its parent liquid (Roeder & Emslie, 1970).

to the surface. Cumulate xenoliths occur also on Easter Island and were found in lava EI9204 near Anakena. These xenoliths consist of large crystals of plagioclase $An_{72–68}$, clinopyroxene $Wo_{45}En_{43}Fs_{12}$ and olivine $Fo_{\sim 71}$ (Tables 2, 3 and 4), which is comparable with the EI9204 phenocrysts (Fig. 2) but much more primitive than the phases in the host basalt matrix (An_{50}). The compositions of the minerals in the xenoliths are also relatively primitive for the subaerial lavas, although Baker *et al.* (1974) found olivines with Fo_{78} in some basalts from the Roiho lava field.

The clinopyroxenes in the samples from Easter Island and the seamounts reflect differences in the chemical composition of the lavas. The clinopyroxenes in most subaerial lavas and in the matrix of many submarine samples are light brown augites, whereas some submarine lavas such as 29DS-2 contain brown clinopyroxenes with sector zoning and anomalous interference colours typical of Ti-augites of alkaline basalts (Table 4). The spinel compositions in the Easter Island and seamount rocks range from Cr-spinel in more primitive basalts to titanomagnetite, whereas ilmenite is the Fe–Ti oxide in sample EI9203 (Table 5). The evolved rocks show a mineralogy typical of trachytic and rhyolitic rocks (Baker *et al.*, 1974). The trachytes appear to be altered by hydrothermal solutions but still contain fayalite, aegirine–augite and

Table 5: Electron microprobe analyses of representative oxide, apatite and amphibole crystals in the Easter Hotspot lavas

Sample:	29DS-2	EI9203	EI9210	EI9210	EI9210
Crystal:	Cr-sp	Ilm	Ti-mt	Ap	Amph
Location:	ol incl.	Matrix	Matrix	ol incl.	Matrix
SiO_2	0·12				34·02
TiO_2	3·22	50·52	20·09		0·61
Al_2O_3	20·69	0·15	0·58		2·98
FeO	30·82	46·43	65·18	1·35	34·02
MnO	0·22	0·49	0·28	0·08	1·22
MgO	11·53	1·57			0·18
CaO				54·59	12·76
Na_2O					0·79
K_2O					0·06
P_2O_5				42·33	
Cr_2O_3	29·82	0·01			
Total	96·44	99·21	86·13	99·92	95·68

tiny green crystals of ferro-hornblende (Table 5; Leake, 1978) as well as patches of quartz and titanomagnetite in their matrix. The fayalite phenocrysts in the trachytes contain tiny inclusions of apatite crystals (Table 5). Many rhyolites are glassy and contain abundant crystallites of feldspar.

Major and trace elements

The $Na_2O + K_2O$ vs SiO_2 diagram of LeBas & Streckeisen (1991) indicates that all basaltic lavas of the subaerial volcanoes have relatively high contents of alkali elements (Fig. 4). Thus, the Easter Island lavas may be classified as tholeiitic to transitional basalts and their differentiates in accordance with earlier results (Baker *et al.*, 1974). The intermediate lavas on Easter Island occur as trachyandesitic lava flows and small volcanic cones on the larger volcano edifices. The most evolved rocks on Easter Island are the trachytes from three parasitic domes of Poike and the rhyolites of Rano Kau, which are shown in Fig. 4. Most samples from the seamounts resemble those from Easter Island in being mildly alkalic basalts and all have SiO_2 contents <50% (Fig. 4). Several of them, such as 43DS-2 and most 25DS samples, are slightly (<1%) nepheline-normative and may thus be classified as alkalic basalts (Table 6). No evolved rocks were recovered from the submarine volcanoes of the Easter Hotspot. Several samples from Pukao seamount are slightly altered and the samples from dredge 33DS and sample 35DS-9 are strongly overprinted by hydrothermal alteration (Table 6) and thus were not plotted. The lavas with the lowest $Na_2O + K_2O$ of the Easter Hotspot are the submarine lavas of 24DS (Rano Kau Ridge) and some samples from dredge 35DS (Pukao seamount) as well as 43DS-1 (unnamed volcanic cone), which are subalkaline tholeiites according to the classification scheme. These lavas resemble the incompatible element enriched tholeiites from the Ahu and Umu volcanic fields further west (Fig. 4). The 24DS and 35DS sample groups are plagioclase cumulates, but microprobe analysis of the 24DS-2 glass confirms the tholeiitic character with low $Na_2O + K_2O$ contents (Table 6). Dredge 43DS taken on a volcanic cone between Moai and Pukao seamounts (Fig. 1) contained two different lava types, where one (43DS-1 and -3) is subalkaline and the other sample is more alkaline. The rocks with low contents of Na_2O and K_2O appear to be restricted to the submarine parts of the Easter Hotspot but are less abundant on the seamounts and the submarine pedestal of Easter Island than the transitional basalts. The wide range of $Na_2O + K_2O$ contents in the basaltic lavas of the Easter Hotspot indicates that probably more than one primary magma existed from which the more evolved lavas differentiated. Lavas which lie along a single liquid line of descent may be defined by using incompatible element ratios, which are not significantly fractionated during crystal fractionation.

Potassium may be leached from subaerial rocks by rainwater alteration (e.g. Feigenson *et al.*, 1983) and thus we use the rare earth elements (REE) to define the different groups of lavas of the Easter Hotspot because they are insensitive to alteration. Each different rock type was analysed for trace elements and a representative data

Table 6: Major element analyses of Easter Island and Pukao Seamount lavas measured by XRF, with the exception of 36DS-4gl by electron microprobe (mp)

Sample:	EI9201	EI9202	EI9203	EI9204	EI9205	EI9206	EI9207	EI9209	EI9210	EI9212	EI9213	EI9214	EI9215	EI9216	EI9217	EI9218	EI9219	BHVO-1
Rock type:	Trn.bas.	Trn.bas.	Trn.bas.	Trn.bas.	Trn.bas.	Haw.	Trn.bas.	Trn.bas.	Trachyte	Trn.bas.	Trn.bas.	Benmor.	Trn.bas.	Trn.bas.	Trn.bas.	Trn.bas.	Rhyolite	
SiO_2	49·88	48·88	48·36	50·09	48·24	53·50	47·70	47·03	67·69	49·16	48·52	58·80	49·29	47·68	47·93	47·74	71·22	49·71
TiO_2	2·976	3·285	3·372	3·283	2·758	2·209	2·762	3·097	0·342	2·959	3·459	1·182	3·187	3·426	3·373	3·378	0·195	2·797
Al_2O_3	14·54	14·70	15·52	14·67	18·22	14·56	16·34	16·44	16·40	16·75	14·97	14·65	15·12	15·01	14·92	14·80	12·70	13·66
$Fe_2O_3^T$	13·35	14·46	14·39	13·94	11·30	13·60	12·31	12·56	5·25	12·17	14·55	11·58	13·56	14·47	14·40	14·14	3·18	12·37
MnO	0·19	0·21	0·20	0·21	0·16	0·24	0·18	0·18	0·12	0·21	0·21	0·26	0·19	0·21	0·20	0·20	0·07	0·17
MgO	5·54	5·33	4·72	4·25	3·70	2·80	7·87	7·14	0·08	4·29	4·77	1·14	5·58	5·91	5·79	5·79	0·00	7·20
CaO	10·09	10·01	9·59	8·80	10·59	6·45	9·90	9·44	0·70	9·94	9·65	4·57	10·17	10·28	10·19	10·29	0·61	11·46
Na_2O	3·27	3·35	3·32	3·74	3·42	4·27	3·02	3·13	6·01	3·50	3·45	5·18	3·04	3·11	3·11	3·13	5·714	2·25
K_2O	0·569	0·392	0·60	0·908	0·491	1·275	0·552	0·586	3·963	0·754	0·672	1·777	0·546	0·282	0·328	0·297	3·789	0·522
P_2O_5	0·364	0·398	0·406	0·508	0·342	1·049	0·365	0·501	0·100	0·387	0·429	0·383	0·363	0·379	0·357	0·380	0·01	0·272
Sum	100·78	100·48	100·48	100·41	99·22	99·96	101·00	100·11	100·66	100·13	100·68	99·524	101·05	100·75	100·44	100·13	97·46	100·41
mg-no.	49·2	46·2	43·3	41·5	43·3	32·4	49·8	57·0	3·4	45·1	43·3	18·7	49·0	48·8	48·4	48·8	0·0	

Sample:	33DS-2	35DS-1a	35DS-1b	35DS-3	35DS-9	36DS-1	36DS-2	36DS-3	36DS-4	36DS-4gl (mp)	37DS-1gl	37DS-4	43DS-1	43DS-1gl	43DS-2	43DS-3
Rock type:	Altered	Tholeiite	Tholeiite	Tholeiite	Altered	Trn.bas.	Alk.bas.	Trn.bas.	Trn.bas.	Trn.bas.	Trn.bas.	Trn.bas.	Tholeiite	Tholeiite	Alk.bas.	Tholeiite
SiO_2	39·75	49·60	49·01	48·17	42·02	47·85	47·72	47·96	47·77	49·50	48·26	48·51	49·16	50·50	48·00	48·89
TiO_2	2·450	2·595	2·661	2·449	4·495	2·409	2·423	2·401	2·45	2·82	2·635	2·684	2·645	2·586	2·559	2·640
Al_2O_3	15·64	17·05	16·30	17·12	15·12	15·37	15·34	15·26	15·32	15·20	16·21	16·83	14·46	13·97	16·15	14·40
$Fe_2O_3^T$	11·45	10·40	11·66	11·02	19·47	11·76	11·75	11·83	11·85	11·78	11·21	11·51	12·66	12·48	11·56	12·66
MnO	0·17	0·14	0·16	0·15	0·30	0·17	0·17	0·17	0·17	0·16	0·17	0·17	0·17	0·17	0·17	0·17
MgO	8·15	5·02	5·48	5·35	5·49	8·75	8·65	8·95	8·58	6·20	6·31	6·61	7·84	7·86	7·92	7·85
CaO	20·36	11·23	11·05	11·34	9·45	9·72	9·76	9·67	9·82	10·40	9·67	9·89	10·18	9·96	10·02	10·18
Na_2O	2·760	3·15	2·97	2·905	3·197	3·00	3·02	3·09	2·98	3·23	3·27	3·35	2·66	2·53	3·06	2·60
K_2O	0·251	0·34	0·352	0·231	0·136	0·551	0·563	0·553	0·614	0·64	0·867	0·907	0·323	0·356	0·766	0·359
P_2O_5	0·475	0·265	0·285	0·285	0·932	0·309	0·305	0·306	0·305	nd	0·398	0·419	0·257	0·250	0·355	0·262
Sum	101·47	99·81	99·94	99·02	100·61	99·88	99·70	100·19	99·87	98·74	99·00	100·88	100·35	100·66	100·56	100·01
norm ne							*0·95*								*0·43*	
mg-no.	62·4	53·0	52·3	53·1	39·7	63·4	63·2	63·8	62·8	55·1	56·8	57·2	59·1	59·5	61·5	59·1

The *mg*-number and the CIPW norms were calculated assuming $FeO = 0{\cdot}85FeO^T$. Most of the lavas are hypersthene-normative but some contain small amounts of normative nepheline which is shown. Trn.bas., transitional basalt; Alk.bas., alkali basalt; Haw., hawaiite; benmor., benmoreite.

Table 6: continued

Sample:	24DS-1	24DS-2	24DS-2gl (mp)	25DS-3	25DS-3gl	25DS-4	26DS-1	26DS-2	27DS-1	27DS-2	27DS-3	27DS-4	27DS-5	29DS-1	29DS-2	29DS-3	29DS-5
Rock type:	Thol.	Thol.	Thol.	Alk.bas.	Alk.bas.	Alk.bas.	Trn.bas.	Trn.bas.	Alk.bas.	Trn.bas.	Alk.bas.	Alk.bas.	Alk.bas.	Trn.bas.	Alk.bas.	Trn.bas.	Trn.bas.
SiO_2	49·15	48·98	50·19	48·17	48·20	48·15	49·77	47·85	47·47	48·06	48·08	47·52	48·18	47·55	48·01	48·02	46·11
TiO_2	1·666	1·680	1·98	3·078	3·038	3·020	2·502	2·441	2·769	2·302	2·879	2·892	2·841	2·76	2·473	2·44	2·93
Al_2O_3	18·72	18·70	14·99	16·37	16·08	16·34	15·02	15·51	15·72	15·62	16·30	16·11	16·10	15·24	15·53	15·64	15·06
$Fe_2O_3^T$	8·57	8·85	10·07	12·21	12·06	12·19	11·80	11·37	12·48	11·42	12·43	12·38	12·56	12·03	11·40	11·20	11·84
MnO	0·13	0·13	0·16	0·17	0·17	0·17	0·18	0·16	0·18	0·17	0·18	0·18	0·18	0·17	0·16	0·16	0·17
MgO	5·99	5·78	7·65	6·13	5·88	6·17	5·88	8·45	7·89	8·70	6·85	6·74	7·44	8·26	8·59	8·41	6·82
CaO	12·46	12·50	11·76	9·55	9·43	9·59	11·02	10·68	9·46	10·16	9·79	9·79	9·64	9·83	10·54	10·53	10·68
Na_2O	2·75	2·83	2·72	3·30	3·38	3·38	3·28	2·79	3·22	2·92	3·22	3·30	3·28	3·00	2·88	2·86	3·03
K_2O	0·343	0·322	0·32	1·052	0·950	1·045	0·532	0·575	0·679	0·585	0·757	0·67	0·73	0·665	0·593	0·589	0·631
P_2O_5	0·178	0·179		0·460	0·447	0·455	0·273	0·302	0·365	0·294	0·376	0·381	0·385	0·382	0·313	0·306	0·404
Sum	99·97	99·96	99·84	100·49	99·64	100·52	100·27	100·13	100·24	100·22	100·85	99·96	101·33	99·89	100·49	100·16	97·67
norm ne				*0·32*		*0·94*			*0·74*		*0·17*	*0·76*	*0·53*		*0·19*		
mg-no.	62·0	60·4	63·9	53·9	53·2	54·1	53·7	63·4	59·6	64·0	56·2	55·9	58·0	61·6	63·7	63·6	57·3

Nepheline normative samples are indicated. Trn.bas., transitional basalt; Alk.bas., alkali basalt.

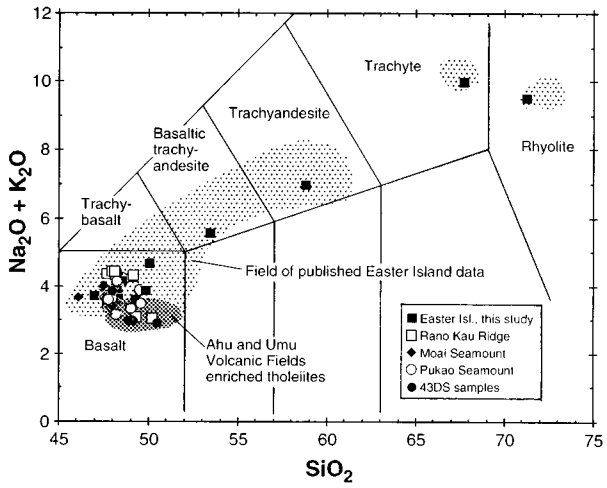

Fig. 4. Total alkali–silica diagram for the classification of volcanic rocks drawn after LeBas & Streckeisen (1991). Also shown are analyses of previously published Easter Island lavas (Baker *et al.*, 1974; Clark & Dymond, 1977; Cheng, 1989) and for the Ahu and Umu volcanic fields close to the spreading axis (Haase & Devey, 1996; Fretzdorff *et al.*, 1996).

set is available (Table 7). Rocks from a single dredge are in most cases very similar and are thus grouped together using the REE content of the representative sample. The REE patterns of all lavas from Easter Island and Rano Kau Ridge are light REE (LREE) enriched and parallel, with the exception of samples EI9209 and 25DS-3gl, which crosscut the patterns of the other lavas (Fig. 5). The lavas from site 24DS on the Rano Kau Ridge are different from the Easter Island lavas, and have lower contents of REE. This is only partly due to plagioclase accumulation because the handpicked, plagioclase-free glass 24DS-4gl shows only slightly higher concentrations than the whole-rock 24DS-1 in Fig. 5a. The rhyolite EI9219 displays the highest REE concentrations and a strong negative Eu anomaly whereas the trachyte EI9210 is relatively depleted in the middle REE (MREE). The samples from the seamounts are also LREE enriched and most lavas display a slight flattening of the patterns between La and Nd (Fig. 5b). Two samples (37DS-1gl and 43DS-2) have relatively straight patterns and these two cross the patterns of the other seamount lavas. The REE patterns of samples from Pukao seamount fan in the LREE although the heavy REE (HREE) are approximately similar (Fig. 5b). The two analysed samples from the unnamed cone also indicate variable compositions, as one lava (43DS-1gl) has the lowest LREE contents in Fig. 5b (La ~40 times chondrite) whereas sample 43DS-2 has high contents of LREE (La ~80 times chondrite) and resembles the most enriched basalt from Pukao seamount.

Figure 6 shows the degree of LREE enrichment vs the MgO contents of the lavas, and on this basis we grouped the samples according to their $(La/Sm)_N$. The most important phenocryst phases occurring in the lavas are olivine and plagioclase, whereas clinopyroxene phenocrysts are found mainly in the more evolved lavas with less than ~5% MgO (Table 1a and b). The fractionation of olivine and plagioclase does not change the ratios of highly incompatible elements (e.g. Nielsen, 1990) and thus we can use, for example, $(La/Sm)_N$ ratios (the subscript N denotes chondrite normalization) to distinguish different magma suites that are not related by fractional crystallization. In Fig. 6 three groups of basalts with >5% MgO can be recognized. The basalts with the highest K_2O contents outlined above (25DS and 37DS) as well as lava 43DS-2 and the two Roiho samples EI9207 and EI9209 show the highest enrichment of the analysed basalts from the Easter Hotspot, with $(La/Sm)_N$ of ~2·2 (Fig. 6). In the following, we will call these relatively enriched lavas the Roiho Group. In contrast, the submarine, mainly tholeiitic basalts 24DS, 43DS-1, 35DS and 26DS-1, are the most depleted lavas from the study area, with $(La/Sm)_N$ of ~1·3. This sample group resembles the incompatible element enriched tholeiites from the Ahu and Umu volcanic fields further west (Fig. 6) and will be called the Volcanic Fields Group in subsequent discussion. The majority of the lavas with >5% MgO have $(La/Sm)_N$ of 1·5–1·9. These include most samples from Easter Island and several samples from Moai and Pukao seamounts. The more evolved lavas from Easter Island have $(La/Sm)_N$ ranging from 1·9 in the trachyandesites to 2·5 in the rhyolite (Fig. 6). Because the basaltic to trachytic lavas from Easter Island appear to form one trend with decreasing MgO the evolved rocks probably formed from a parental magma from this intermediate suite, which we will call the Main Group.

In Fig. 7 we show the major element variations of the Easter Hotspot lavas vs MgO. The three groups defined above have comparable trends for most major elements. However, the Volcanic Fields Group generally has lower Na_2O, K_2O, P_2O_5 and TiO_2 contents at a given MgO than the other two lava groups. On the other hand, this group has the highest CaO and appears to be slightly higher in SiO_2. The Roiho group generally has the highest K_2O and P_2O_5 contents but is otherwise similar to the Main Group. The range of MgO contents of all seamount lavas lies between 9 and 4·5%, and is higher than for most Easter Island rocks (8 to ~0%, Table 6), in accordance with the observation that no evolved lavas were recovered from the submarine volcanoes. The field of the published data on Easter Island lavas is shown and follows the trend of our samples but displays a much wider range. The trends of the major elements vs MgO of Main Group lavas display two major changes (Fig. 7). Between 8 and ~5% MgO, all major elements have approximately constant or increasing concentrations. The

Table 7: Trace element concentrations (in p.p.m.) of Easter Island samples, from Rano Kau Ridge (24DS and 25DS), the cone between Moai and Pukao seamounts (43DS), and Moai and Pukao Seamounts (26DS–29DS and 35DS–37DS, respectively); also given is the average of USGS standard BHVO-1 which was measured ten times together with the samples over a period of 2 years

Sample:	EI9201	EI9204	EI9206	EI9207	EI9209	EI9210	EI9214	EI9216	EI9218	EI9219	24DS-1	24DS-4gl	25DS-3gl	43DS-1gl	43DS-2gl	26DS-1	27DS-1	27DS-2	27DS-4	29DS-1	35DS-1a	36DS-1	36DS-4gl	37DS-1gl	BHVO-1
Sc	33·2	29·3	17·2	27·9	22·0	4·00	17·1	36·3	35·0	4·48	27·0	28·0	28·2	27·9	23·1	36·9	26·7	28·6	28·1	25·9	28·2	26·1	25·0	27·4	31·8±3·2
V	366	419	86·2	294	306		11·8	396	299	18·7	218	295	342	291	278	340	283	267	296	262	274	259	288	303	392±49
Cr	22·2	32·7	1·00	209	156		1·24	107	89·3	0·0	238	330	119	364	188	167	174	306	151	292	153	288	269	156	316±28
Co	38·9	33·5	16·3	48·3	37·4	5·10	3·59	46·3	33·2	0·02	33·1	36·1	36·4	45·4	38·8	40·1	43·8	46·1	40·6	46·1	36·8	45·9	42·8	37·5	44·0±2·4
Ni	31·3	18·6	0·69	139	105	2·8	0·01	42·8	37·1	5·88	77·4	76·8	80·0	143	124	52·7	157	174	94·9	171	56·7	176	155	84·9	118±6
Cu	54·6	37·8	15·67	49·9	33·2	7·2	5·21	49·7	36·2	3·37	61·2	61·2	60·1	71·3	39·8	74·7	48·3	57·1	51·7	47·8	70·7	48·0	42·0	58·4	137±13
Zn	134	111	121	99·8	84·7	196	135	113	115	169	71·9	62·7	135	127	69·7	105	109	90·3	101	101	96·7	92·7	76·7	122	107±22
Y	36·1	51·9	76·0	37·1	39·0	59·4	85·2	39·0	35·2	122	20·4	23·0	35·7	27·1	26·3	36·7	35·5	29·9	36·8	33·3	29·4	29·6	31·9	32·8	25·7±0·8
Rb	8·31	10·8	22·9	5·54	3·66	85·4	28·3	1·91	0·55	62·0	3·85	2·58	17·4	4·66	11·8	3·67	9·38	9·04	9·85	9·58	4·24	7·67	7·04	15·0	9·23±0·78
Cs	0·10	0·11	0·24	0·03	0·03	0·165	0·325	0·019		0·676	0·05	0·03	0·24	0·06	0·13	0·17	0·12	0·10	0·12	0·12	0·06	0·10	0·08	0·16	0·09±0·05
Sr	259	266	231	318	300	57	209	275	264	22·8	254	205	336	200	305	226	269	278	283	321	273	277	263	332	375±31
Ba	108	151	198	119	148	492	265	106	90·1	378	32·2	35·1	152	41·3	120	54·9	97·4	88·9	99·0	93·6	48·7	75·3	71·5	133	122±7
Zr	211	374	555	191	272	1355	672	219	191	638	94·3	119	250	145	175	164	206	163	211	212	149	157	194	227	172±5
Hf	5·33	7·05	9·34	4·57	5·44	29·3	14·0	5·19	5·25	21·8	2·23	2·65	5·56	3·77	3·88	4·09	4·87	4·05	5·09	5·23	3·79	3·99	4·16	4·86	4·09±0·42
Nb	25·7	39·6	48·5	26·9	37·3	130	64·1	27·3	22·4	94·1	8·00	9·94	40·7	14·1	28·6	13·4	20·4	19·4	21·9	22·6	14·7	17·6	18·1	36·2	17·2±1·5
Ta	1·73	2·47	2·92	1·62	2·34	7·35	3·89	1·58	1·57	6·31	0·54	0·69	6·99	0·97	1·88	0·90	1·32	1·25	1·40	1·46	0·98	1·08	1·21	1·94	1·04±0·20
Pb	1·08	1·65	2·15	1·16	1·38	5·95	2·85	1·16	1·09	6·56	0·44	0·68	1·44	0·63	1·21	0·86	1·09	1·03	1·24	1·22	0·78	0·99	0·98	1·31	2·00±0·15
Th	1·69	3·16	3·95	1·50	2·90	15·4	5·60	1·46	1·80	11·4	0·42	0·60	2·37	0·76	2·32	0·82	1·39	1·22	1·43	1·32	0·82	0·98	1·29	1·97	1·02±0·09
U	0·47	0·92	1·27	0·56	0·85	3·52	1·90	0·26	0·24	3·27	0·18	0·23	0·77	0·28	0·70	0·34	0·52	0·45	0·53	0·54	0·50	0·43	0·48	0·62	0·42±0·02
La	17·7	28·2	40·5	21·6	29·4	71·3	49·6	17·8	17·6	82·6	6·18	7·15	24·9	9·25	19·3	11·0	16·1	13·6	16·4	16·2	10·4	12·7	13·6	21·9	14·4±0·69
Ce	41·6	73·4	113·3	45·5	72·6	163	127	42·9	41·5	181	16·3	20·5	55·4	23·3	47·2	28·1	39·3	32·7	40·1	40·4	26·5	32·0	37·5	48·8	36·6±1·6
Pr	5·43	8·85	13·3	6·09	8·57	21·4	15·4	5·77	5·37	21·2	2·42	2·83	7·00	3·32	5·70	4·14	5·44	4·48	5·45	5·62	3·81	4·51	4·95	6·29	5·16±0·28
Nd	25·4	37·6	57·8	26·8	35·5	85·5	64·8	25·8	24·6	84·8	11·5	13·3	29·7	16·6	23·5	19·5	24·7	20·2	24·7	25·7	18·1	20·3	22·1	26·5	23·7±1·29
Sm	6·58	9·21	14·1	6·34	8·17	21·6	15·5	6·72	6·75	20·9	3·28	3·77	7·05	4·58	5·53	5·54	6·28	5·26	6·37	6·71	5·04	5·30	5·77	6·28	6·01±0·45
Eu	2·22	2·85	4·14	2·13	2·59	5·85	4·81	2·28	2·25	3·19	1·22	1·36	2·18	1·64	1·84	1·91	2·13	1·82	2·13	2·24	1·80	1·78	1·96	2·07	1·98±0·07
Gd	7·28	9·97	15·0	6·73	8·55	22·0	16·4	7·27	7·14	21·1	3·58	4·38	7·41	5·26	5·75	6·23	6·66	5·56	6·76	6·88	5·39	5·50	6·36	6·64	6·04±0·30
Tb	1·13	1·51	2·25	1·01	1·25	3·93	2·55	1·14	1·15	3·66	0·50	0·70	1·05	0·84	0·87	1·04	1·07	0·89	1·07	1·05	0·89	0·87	0·98	0·95	0·89±0·07
Dy	6·80	8·82	13·0	5·92	7·07	25·5	14·9	6·71	7·12	22·8	3·57	4·24	6·14	5·15	4·96	6·33	6·30	5·37	6·58	6·17	5·28	5·16	5·77	5·69	5·00±0·40
Ho	1·29	1·64	2·38	1·16	1·29	5·30	2·78	1·29	1·35	4·57	0·72	0·79	1·18	0·95	0·90	1·29	1·25	1·05	1·28	1·56	1·04	1·02	1·08	1·09	0·91±0·07
Er	3·73	4·94	7·05	3·21	3·70	16·9	8·53	3·55	3·83	13·5	2·00	2·36	3·37	2·70	2·64	3·71	3·49	2·91	3·59	3·19	2·82	2·82	3·22	3·06	2·38±0·13
Tm	0·50	0·65	0·91	0·42	0·48	2·80	1·15	0·49	0·51	1·88	0·28	0·31	0·44	0·35	0·35	0·51	0·50	0·39	0·48	0·42	0·38	0·38	0·42	0·41	0·30±0·02
Yb	3·21	4·22	5·90	2·76	3·13	21·1	7·73	3·14	3·13	12·5	1·69	1·96	2·98	2·31	2·23	3·20	3·05	2·57	3·18	2·64	2·42	2·60	2·73	2·70	1·92±0·14
Lu	0·47	0·59	0·81	0·38	0·43	3·15	1·07	0·43	0·48	1·74	0·25	0·27	0·41	0·32	0·31	0·47	0·45	0·36	0·45	0·37	0·34	0·36	0·38	0·37	0·26±0·02
$(La/Sm)_N$	1·74	1·98	1·85	2·20	2·32	2·13	2·06	1·71	1·68	2·55	1·22	1·22	2·28	1·30	2·25	1·28	1·66	1·67	1·66	1·56	1·33	1·55	1·52	2·25	

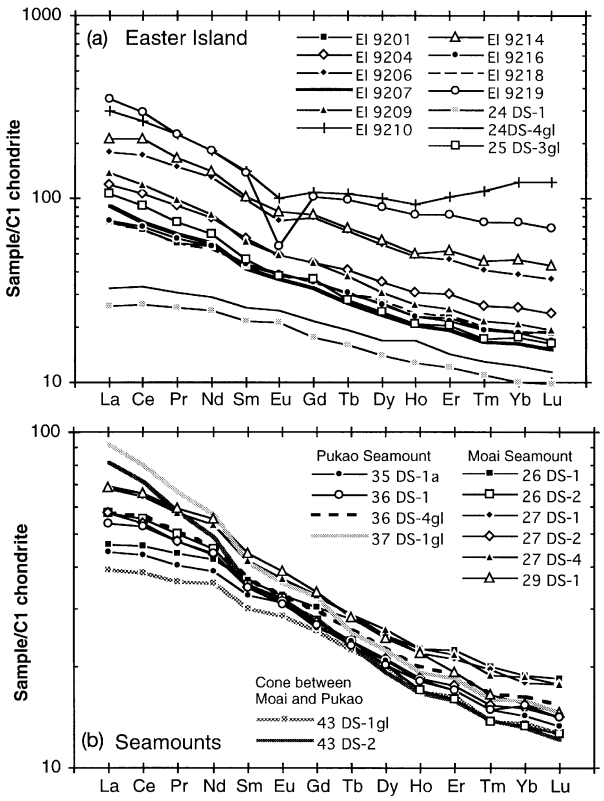

Fig. 5. C1 chondrite-normalized REE diagrams (a) for samples from Easter Island and Rano Kau Ridge and (b) samples from Moai and Pukao Seamounts as well as from the unnamed cone between the two seamounts. Chondrite from Sun & McDonough (1989).

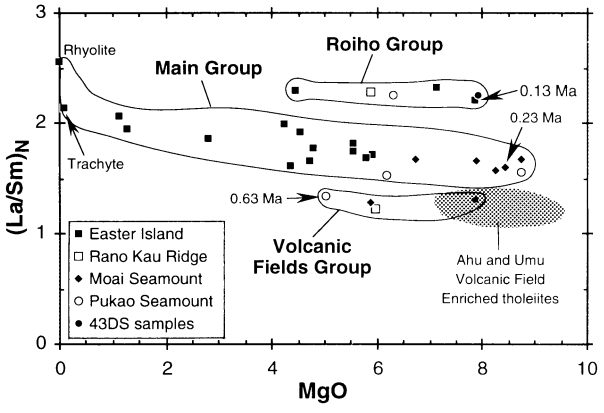

Fig. 6. Plot of $(La/Sm)_N$ vs MgO for the Easter Hotspot lavas in comparison with the enriched volcanic field tholeiites. Because of the similarities of the relatively depleted lavas described in this paper to the enriched tholeiites from the volcanic fields further to the west these rock are called 'Volcanic Fields Group', whereas the other two groups are more enriched. The three age dates are from O'Connor *et al.* (1995), and may indicate a temporal evolution through three chemically distinct volcanic stages in the Easter Hotspot. Six analyses of Easter Island lavas are from Bonatti *et al.* (1977) and volcanic fields data are from Haase & Devey (1996).

first change of the trends occurs at ~5% MgO, where TiO_2 and CaO, and to a lesser extent FeO^T, begin to decrease with falling MgO (Fig. 7). SiO_2 and K_2O increase at MgO contents lower than 5%, whereas P_2O_5 rises from 0·4% to 1% between 5 and 3% MgO before falling sharply. The second strong change in trend appears to take place at ~2% MgO, leading to a stronger decrease of FeO^T and a steeper increase in SiO_2 and K_2O. Lavas from Pinzon Island in the Galapagos Archipelago (Baitis & Lindstrom, 1980) and of Austurhorn volcano on Iceland (Furman *et al.*, 1992) follow the same trends (Fig. 7). The plagioclase cumulates of 24DS deviate significantly from the trend of the Easter Hotspot samples (for instance, to much higher Al_2O_3 contents) whereas the 24DS-2 glass is a relatively primitive sample in the Volcanic Fields Group. The observed high Al_2O_3 values of some Easter Island samples and samples from Pukao seamount (35DS-1) are related to varying degrees of plagioclase accumulation because they follow the vectors of the 24DS samples (Fig. 7).

There is a good agreement between the enrichment observed in the LREE and other incompatible elements such as K or P, and the definition of three groups of lavas appears valid (Fig. 7). The basalts from 25DS (Rano Kau Ridge), 37DS (Pukao) and 43DS-2 have the highest K_2O contents of ~0·8–1·0%. However, the two Roiho Group lavas from Easter Island (EI9207 and EI9209) have lower K_2O contents, which might indicate some K loss owing to alteration. The rest of the basalts from Easter Island and most primitive lavas from the seamounts have slightly lower contents of K_2O than the extreme samples of 25DS and 37DS, whereas the lowest K_2O contents are found in the glass 24DS-2 and samples 43DS-1 and -3.

DISCUSSION

Crystal fractionation

Determination of crystallizing phases and least-squares modelling

As we have shown above, a variety of rock types occurs on Easter Island and the neighbouring seamounts. The variation within each of the defined lava groups is attributed to crystal fractionation or accumulation processes at relatively shallow levels. Nielsen (1990) has shown that the $(La/Sm)_N$ ratio is only slightly changed during crystal fractionation of the common phases olivine, plagioclase and Fe–Ti oxides, whereas voluminous clinopyroxene fractionation may lead to an increase of the ratio. Thus, the variations in the incompatible element enrichments in the basaltic magmas (the most primitive lavas in each suite have ~8% MgO) must have formed either by different partial melting processes or from differences in the source compositions. These processes will be discussed

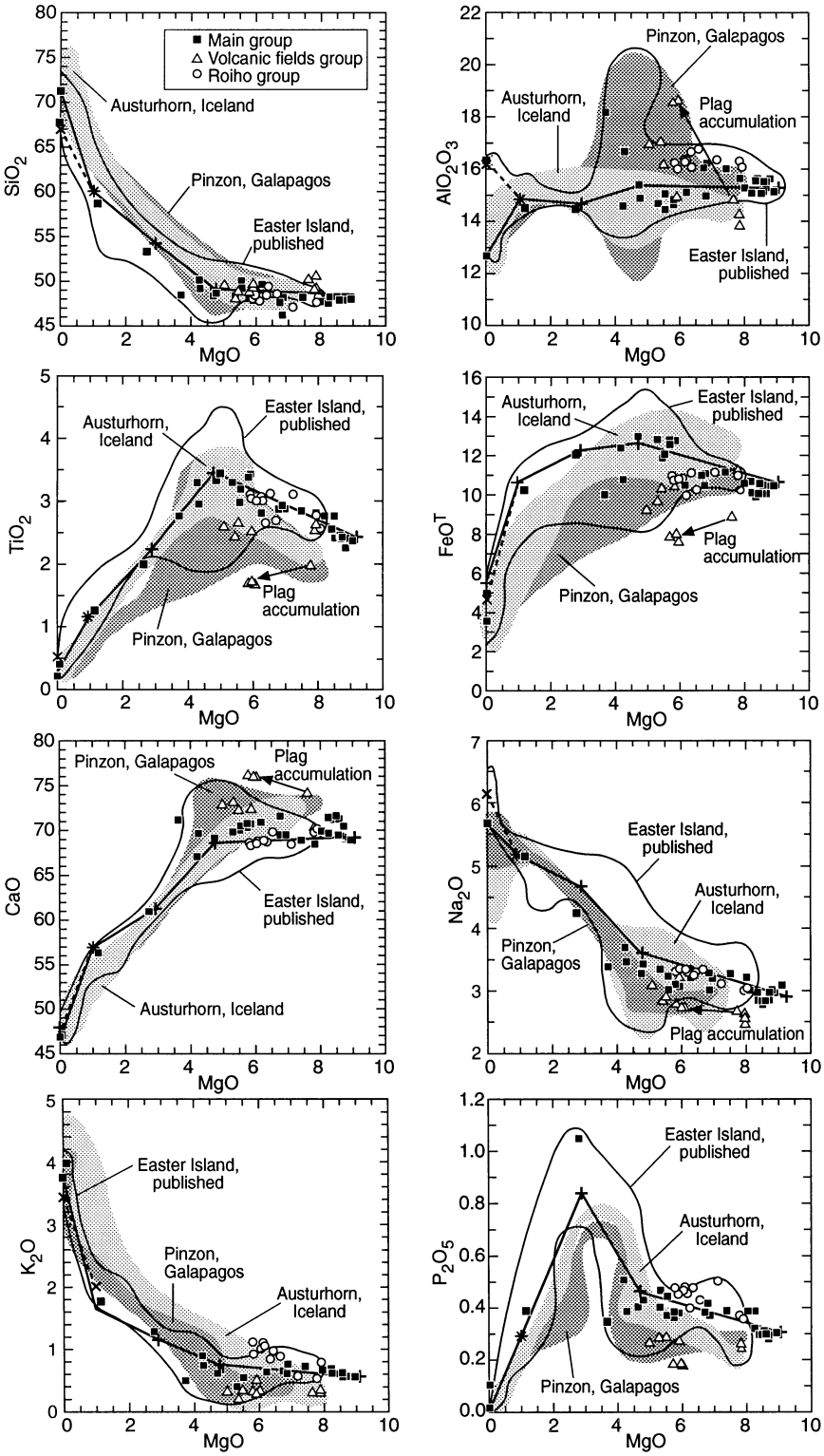

Fig. 7. Major element diagrams for the lavas with an outline of the field for published analyses of Easter Island lavas from Baker *et al.* (1974) and Clark & Dymond (1977). The light grey field shows the trend of the Austurhorn rocks from Iceland (Furman *et al.*, 1992), and the dark grey field the lavas from Pinzon Island in the Galapagos (Baitis & Lindstrom, 1980) is also included. The lines connect least-squares calculated daughter liquids of the Main Group lavas.

later after the role of fractional crystallization in the petrogenesis of the evolved rocks has been investigated.

Although not all magmas of the Easter Hotspot have formed from the same parental magma by crystal fractionation, most samples fall on similar trends on the major element variation diagrams. The relatively constant trends of all elements between 9 and 5% MgO indicate a fractionation assemblage of olivine, plagioclase and clinopyroxene, which are the only phenocrysts present in the more primitive lavas (Table 1a and b). The generally constant trend of the Main Group lavas from basalts to the trachyandesitic rocks with ~1% MgO indicates a constant fractionation of the Al_2O_3-rich phase plagioclase. The high Al_2O_3 in several Main Group basalts with 3–7% MgO probably implies some plagioclase accumulation, an abundant feature in the published Easter Island (and Pinzon) lavas which leads to the very high Al_2O_3 contents in Fig. 7. The crystal fractionation of the magmas of the Main Group was modelled using the GPP least-squares calculation program of Geist *et al.* (1985). The fractionation was calculated in four steps using a sample analysis at each change of the trend as parent composition for the next step. The most mafic basalt, 36DS-3, with ~9% MgO, was taken as the parental magma, but we used an average Na_2O content of 2·95% of the 36DS lavas because 36DS-3 has an extremely high Na_2O content. The lines in Fig. 7 connect the calculated liquids, and the fit to the Main Group trend is good, as are the squared residuals (Table 8). We used analysed mineral compositions for the fractionating assemblage and change the compositions in each step. For instance, the first fractionation assemblage consists of phases in the gabbroic xenoliths on Easter Island occurring in lava EI9203, the daughter analysis of the first step. The good fit indicates that the cumulate xenoliths probably formed from a primitive magma comparable with 36DS-3 giving rise to the relatively evolved basalts of Easter Island. In basalts with >5% MgO olivine is more prominent than clinopyroxene but plagioclase is the dominant fractionating phase in accordance with the modal abundances (Table 1). Following the first step (at MgO <5%) clinopyroxene becomes more important than olivine in the fractionating assemblage, leading to the strong CaO decrease (Fig. 7 and Table 8). However, olivine fractionation continues through the whole range of magma compositions and in the most evolved lavas (trachytes and rhyolites) fayalitic olivine crystallizes. The fractionation of Fe–Ti oxides leads to the decreasing TiO_2 and to a lesser degree FeO^T. At ~3% MgO apatite joins the fractionation assemblage and changes the trends for P_2O_5 and SiO_2. In the lavas with <1% MgO the Al_2O_3 contents change significantly; the rhyolites display a decrease in Al_2O_3 whereas the trachytes have slightly increased Al_2O_3 contents relative to the basalts. The lower SiO_2 content of the trachytes compared with the rhyolites suggests either less fractionation or the enhanced fractionation of a phase high in SiO_2. The modelling indicates that the rhyolites require the fractionation of large volumes of plagioclase and K-feldspar, which is significantly less in the trachytes (Table 8). Comparable differences in the volumes of K-feldspar fractionation and the important role of K-feldspar in the resulting SiO_2 contents of evolved lavas were suggested by Wilson *et al.* (1995).

Figure 7 shows that volcanoes of the Galapagos and Iceland hotspots follow similar fractionation trends to the Easter Island lavas. For instance, the change from Ti and Fe enrichment with decreasing MgO to Fe–Ti depletion occurs at ~5% MgO in all three magma series (Fig. 7). The point of apatite saturation is reached in all three cases at ~0·8% P_2O_5 and 3·0–3·5% MgO, which is also comparable with another Galapagos volcano, Alcedo (Geist *et al.*, 1995). These similarities suggest comparable fractionation processes occurring in all three regions and possibly in many other volcanoes generated close to a spreading axis.

In the Roiho Group the fractionation can be modelled with dominantly olivine, clinopyroxene and spinel fractionation whereas plagioclase is subdued (Table 8). The differences observed in the Volcanic Fields Group are mainly due to plagioclase accumulation in lavas 35DS and 24DS. Calculations suggest that ~5% olivine fractionation and 17% plagioclase accumulation can change the composition from the primitive glass 43DS-1gl to sample 35DS-1a (Table 8). The abundance of plagioclase cumulates among the rocks of this group and among the more evolved lavas on Easter Island is probably due to the low density contrasts between the melts and the crystals, which inhibit the fractionation of plagioclase (e.g. Kushiro, 1980). Similar plagioclase-rich rocks are frequently observed in the Galapagos and on Iceland (Cullen & McBirney, 1987; Macdonald *et al.*, 1990; Geist *et al.*, 1995).

The formation of the trachytes and rhyolites

The trachytes and the rhyolites have high contents of incompatible elements such as K and La requiring extremely large amounts of fractionation (>85%). An alternative explanation for the generation of Icelandic rhyolites by remelting of amphibolite facies basaltic crust was suggested, for example, by O'Nions & Grönvold (1973) and Oskarsson *et al.* (1982). This model is supported by the very low $\delta^{18}O$ values of many Icelandic siliceous rocks (e.g. Condomines *et al.*, 1983), which can be explained most easily by melting or high degrees of assimilation of altered crust. However, we suggest that the Easter Island rhyolites formed by crystal fractionation processes for several reasons. First, although basalts are the most abundant rocks on Easter Island there is a

Table 8: Results of the least-squares crystal fractionation calculations for the three groups of samples found at the Easter Hotspot (see text for discussion)

	SiO_2	TiO_2	Al_2O_3	FeO^T	MnO	MgO	CaO	Na_2O	K_2O	P_2O_5
Main Group										
36DS-3	48·44	2·42	15·41	10·75	0·17	9·04	9·77	3·12	0·56	0·31
−11·1% Ol	40·34			13·95	0·20	46·15	0·30			
−5·0% Cpx	50·46	1·40	3·49	7·48	0·15	14·71	21·51	0·43		
−15·8% Plag	51·81		29·77	0·60		0·14	13·98	3·92	0·14	
Calc.	49·01	3·46	15·52	12·85	0·21	4·72	9·50	3·49	0·78	0·46
EI9203	48·83	3·40	15·67	13·07	0·20	4·77	9·68	3·35	0·61	0·41
	$\Sigma R^2 = 0{\cdot}195$									
EI9203	48·83	3·40	15·67	13·07	0·20	4·77	9·68	3·35	0·61	0·41
−6·4% Ol	35·51			37·62	0·59	26·34	0·33			
−12·8% Cpx	50·07	1·39	2·47	13·14	0·31	12·35	19·70	0·49		
−26·4% Plag	50·92		30·71	0·62		0·12	14·77	3·65	0·10	
−1·4% Ti-mt		20·09	0·58	65·18	0·28					
−3·5% Ilm		50·52	0·15	46·43	0·49	1·57	0·17			
Calc.	54·21	2·24	14·74	12·41	0·21	2·88	6·58	4·72	1·17	0·84
EI9206	54·26	2·24	14·77	12·41	0·24	2·84	6·54	4·33	1·29	1·06
	$\Sigma R^2 = 0{\cdot}225$									
EI9206	54·26	2·24	14·77	12·41	0·24	2·84	6·54	4·33	1·29	1·06
−7·0% Ol	35·51			37·62	0·59	26·34	0·33			
−1·8% Cpx	50·18	1·38	1·70	17·62	0·39	9·58	18·91	0·54		
−11·4% Plag	50·92		30·71	0·62		0·12	14·77	3·65	0·10	
−2·7% Ilm		50·52	0·15	46·43	0·49	1·57	0·17			
−1·8% Ap				1·40			54·00			42·30
Calculated	59·97	1·10	14·97	10·75	0·24	1·01	4·67	5·19	1·71	0·38
EI9214	59·78	1·20	14·89	10·59	0·26	1·16	4·65	5·27	1·81	0·39
	$\Sigma R^2 = 0{\cdot}113$									
−6·4% Ol	29·73			65·89	2·46	0·44	0·63			
−11·3% Cpx	49·44	1·99	2·36	15·61	0·32		19·97	0·21		
−11·3% Plag	52·48		29·25	0·71		0·13	13·59	4·20	0·16	
−45·6% K-fsp	67·89		21·29	0·18	0·00		2·00	7·74	1·83	
−3·9% Ti-mt	0·51	20·69	0·58	65·18	0·28					
−0·9% Ap				1·40			54·00			42·30
Calculated	71·25	0·22	12·68	5·62	0·22	–0·04	0·64	5·76	3·73	–0·03
EI9219	71·27	0·20	12·71	5·63	0·07	0·00	0·61	5·71	3·79	0·01
	$\Sigma R^2 = 0{\cdot}038$									
EI9214	59·78	1·20	14·89	10·59	0·26	1·16	4·65	5·27	1·81	0·39
−5·3% Ol	29·73			65·89	2·46	0·44	0·63			
−13·5% Cpx	50·18	1·38	1·70	17·62	0·39	9·58	18·91	0·54		
−3·5% Plag	52·48		29·25	0·71		0·13	13·59	4·20	0·16	
−34·7% K-fsp	67·89		21·29	0·18	0·00		2·00	7·74	1·83	
−3·7% Ti-mt	0·51	20·69	0·58	65·18	0·28					
−1·0% Ap				1·40			54·00			42·30
Calculated	67·18	0·41	16·34	4·73	0·18	–0·43	0·88	6·19	3·64	–0·12
EI9210	67·67	0·34	16·38	4·71	0·12	0·08	0·70	6·00	3·96	0·10
	$\Sigma R^2 = 0{\cdot}800$									
Roiho Group										
43DS-2	48·28	2·58	16·25	10·46	0·17	7·97	10·08	3·08	0·77	0·36
−3·1% Ol	40·34			13·95	0·20	46·15	0·30			
−4·3% Cpx	50·46	1·40	3·49	7·48	0·15	14·71	21·51	0·43		
−1·7% Plag	51·81		29·77	0·60		0·14	13·98	3·92	0·14	
−4·1% Cr-sp		3·22	20·69	30·82	0·22	11·53				
Calculated	49·23	2·80	16·55	10·27	0·18	6·45	9·88	3·34	0·89	0·42
37DS-1gl	49·30	2·70	16·56	10·30	0·17	6·45	9·88	3·34	0·89	0·42
	$\Sigma R^2 = 0{\cdot}018$									
Volc. Fields Group										
43DS-1	49·61	2·67	14·59	11·50	0·17	7·91	10·27	2·68	0·32	0·26
−4·9% Ol	40·34			13·95	0·20	46·15	0·30			
+16·7% Plag	51·81		29·77	0·60		0·14	13·98	3·92	0·14	
Calculated	50·34	2·39	17·50	9·76	0·14	5·07	11·26	2·99	0·31	0·23
35DS-1a	50·22	2·63	17·26	9·48	0·14	5·08	11·37	3·19	0·34	0·27
	$\Sigma R^2 = 0{\cdot}263$									

continuous differentiation trend of more evolved lavas towards the trachytes and rhyolites (Figs 4 and 7). The most evolved rocks probably formed from a Main Group parent because this group is most abundant on Easter Island and apparently forms the parental magmas for the intermediate rocks. This is confirmed by the good results of the least-squares (sum $R^2 \ll 1$, Table 8) major element modelling of the Easter Island rhyolites and trachytes. Second, the rhyolites and trachytes are the products of Rano Kau and Pukao volcanoes, which consist only of lavas from the Main Group. Third, Taylor (1968) has shown that some Easter Island rhyolites have $\delta^{18}O$ values of ~6‰ SMOW (Standard Mean Ocean Water), which could be explained by strong fractionation (>90%) of a basalt with an initial $\delta^{18}O$ of ~5·5‰ SMOW (Taylor & Sheppard, 1986). Finally, the Sr and Nd isotopic composition of rhyolite EI9219 (0·702993 ± 9 and 0·512988 ± 9, respectively) is similar to that of the Main Group basalts of Easter Island (Haase *et al.*, 1996; Fig. 8a). Oceanic crust is hydrothermally altered by seawater shortly after its generation at the spreading axis and has high $^{87}Sr/^{86}Sr$ (Hart & Staudigel, 1989). The $^{87}Sr/^{86}Sr$ values of the unleached samples from Easter Island are higher for a given Nd isotope ratio than are the analyses of the leached lavas (Fig. 8a), thus indicating that even the very young lavas (<0·5 Ma) are seawater contaminated. A melt from such an altered crust would inherit the higher Sr and lower O isotopic ratio, which is not observed in the rhyolite. Although the Easter Hotspot is underlain by oceanic crust with an enriched composition (Hanan & Schilling, 1989; Haase *et al.*, 1996), the composition of this crust is less radiogenic in Sr and more radiogenic in Nd than the rhyolite and the trachyte. Thus, any magma formed from this unaltered oceanic crust should have the isotopic composition of MORB, which is also not observed.

The modelling of the fractionation assemblage leading to the rhyolites and trachytes suggests a total crystallization of 74% and 62%, respectively, of the phases plagioclase, K-feldspar, fayalite, clinopyroxene, Ti-magnetite and apatite to generate a rhyolite from a trachyandesite with ~1·1% MgO, which is comparable with the fractionation models of the Austurhorn volcano on Iceland (Furman *et al.*, 1992). Because we infer that both trachytes and rhyolites formed from a parent magma of the Main Group, their evolution to different compositions must have occurred rather late in the fractionation process. The modelling results for the trachyte are improved if the parent trachyandesite with 1·1% MgO has a higher K_2O content than for the parent of the rhyolite (Fig. 7 and Table 8). The trachyandesitic rocks on Easter Island show a large variation in K_2O and thus a relatively K-rich parent for the trachytes is plausible. Most importantly, the least-squares calculations have shown that the main difference is the much larger volume of plagioclase and

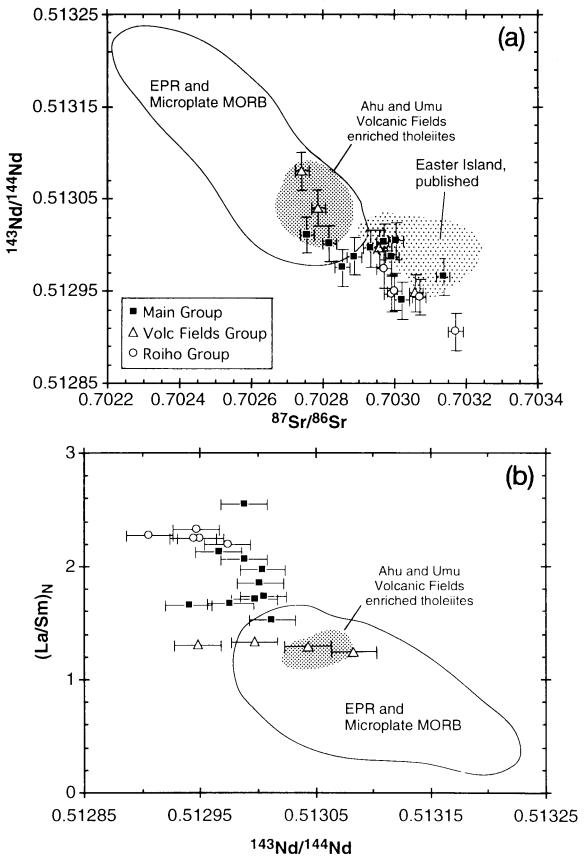

Fig. 8. (a) Strontium vs Nd isotope compositions with error bars of the Easter Hotspot lavas compared with fields for the Volcanic Fields lavas and East Pacific Rise and Microplate MORB. Also shown is the field for published Easter Island data, which are slightly removed to higher $^{87}Sr/^{86}Sr$ possibly as a result of seawater alteration, as many of these samples were not leached. (b) $(La/Sm)_N$ vs $^{143}Nd/^{144}Nd$ for the three groups indicating some compositional overlap between the groups. Data are from White & Hofmann (1982), Macdougall & Lugmair (1986), White *et al.* (1987), Cheng (1989), Bach *et al.* (1994), Mahoney *et al.* (1994), Haase (1995) and Haase *et al.* (1996).

K-feldspar fractionation required to generate the rhyolites. This difference can also be observed in trace elements such as Eu and Sr, because Eu shows a strong negative anomaly in the rhyolites compared with the trachytes (Fig. 5). Whereas the Eu/Eu* value is relatively constant in the basaltic lavas and the trachytes from Easter Island, the rhyolites have low Al_2O_3, Eu/Eu* and Sr (Fig. 9). The basalts and the rhyolites lie within the Austurhorn trend in Fig. 9, suggesting similar fractionation assemblages. The higher Al_2O_3 and Sr contents of the trachyte EI9210 than the rhyolite EI9219 (Fig. 9) are due to stronger feldspar fractionation in the petrogenesis of the rhyolites (clinopyroxene/feldspar ratio ~0·20), whereas clinopyroxene crystallization is more important during the generation of the trachytes (clinopyroxene/feldspar ratio ~0·35, Table 8). Although more

clinopyroxene fractionates to form the trachytes, the Sc contents of the trachytes are only slightly lower than those of the rhyolites (Table 7). The trachyte also does not show the enrichment of the LREE relative to the MREE suggested by Nielsen (1990) and Geist *et al.* (1995) for extensive clinopyroxene fractionation, whereas the rhyolite has elevated $(La/Sm)_N$(Fig. 6). The determination of the distribution coefficients of Ba and Rb in plagioclase has shown $D^{Ba/Rb}>1$ (Philpotts & Schnetzler, 1970; Hart & Brooks, 1974) and thus Ba/Rb should be significantly fractionated in the rhyolites, which is indeed the case (~6 compared with Ba/Rb of 10–15 for basalt glasses). The different volumes of plagioclase and K-feldspar in the fractionation assemblages may be due to either higher pressures of fractionation or an increased water content in the trachytic magmas, both of which inhibit feldspar crystallization (Yoder & Tilley, 1962; Holloway & Burnham, 1972; Presnall *et al.*, 1979). A higher water content in the trachytes than in the rhyolites is supported by the presence of amphibole in the former. However, a higher pressure fractionation origin of the trachyte magmas cannot be ruled out.

Inferences on the depths of fractionation

Whereas the submarine lavas are comparatively mafic, with MgO >5%, the volcanics from Easter Island span a large range in compositions from basalts to trachytes and rhyolites, most lavas having MgO contents between 5 and 3% MgO (Baker *et al.*, 1974). Such an abundance of evolved lavas occurs frequently on islands on relatively young oceanic crust (3–15 Ma) such as Bouvet (Imsland *et al.*, 1977), Pitcairn (Woodhead & McCulloch, 1989) or Ascension (Harris, 1983), but is also observed in the alkaline lavas of Hawaiian volcanoes in the late shield and in the post-shield stages (e.g. Spengler & Garcia, 1988). The abundance of the evolved lavas may be related to a waning magma supply rate or due to the effect of elevation of the islands, which prevents the ascent of mafic magmas to the surface. The most evolved rocks on Easter Island occur at the end of magmatic activity of each volcano, which is comparable with both Hawaii (Spengler & Garcia, 1988; Frey *et al.*, 1990) and the Galapagos Archipelago (Geist *et al.*, 1995). The formation of these more evolved magmas is probably due to the decreasing magma supply, which allows extensive fractionation without replenishment by mafic magmas. However, even the relatively young Terevaka volcano consists mainly of relatively evolved basalts (average $4{\cdot}58 \pm 1{\cdot}61\%$ MgO; $n=37$; Baker *et al.*, 1974; Cheng, 1989; this work), which are significantly less mafic than the submarine seamount lavas (average $7{\cdot}47 \pm 1{\cdot}19\%$ MgO; $n=29$). Thus, the higher elevation of the subaerial volcanoes relative to the submarine may inhibit the ascent of large volumes of mafic magmas because they have to

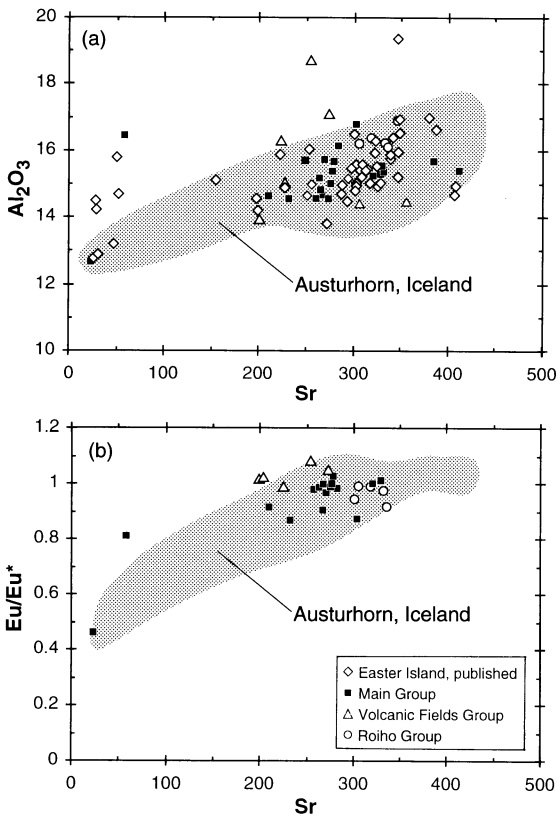

Fig. 9. (a) Al_2O_3 vs Sr contents for the Easter Hotspot lavas and (b) Eu/Eu* vs Sr [Eu* calculated as $(Sm_N+Gd_N)/2\times 0{\cdot}058$], showing that the Easter basalts and the rhyolites lie within the field of the Austurhorn rock suite on Iceland. Published data are from Baker *et al.* (1974), Cheng (1989) and Austurhorn from Furman *et al.* (1992).

rise through a shallow compensation level of buoyancy (e.g. Sinton & Detrick, 1992). Submarine Hawaiian lavas also appear to be more mafic than the subaerial rocks even during the shield stage of the volcano when the magma supply rate is high (Clague *et al.*, 1991). Easter Island is only ~1000 m higher than the seamounts, but it appears that this small difference in elevation results in more extreme fractionation. This would imply a very shallow level magma reservoir (perhaps in the uppermost 2 km) in which a large part of the fractionation occurs and where the evolved basalts and the trachybasalts of Easter Island form. However, crystallization must start at deeper levels, as is indicated by the presence of large pheno- and xenocrysts in the submarine lavas. Ryan (1993) suggested that the location of a horizon of neutral buoyancy controls the position of magma chambers, which he estimated to lie between 1 and 3 km for picritic and tholeiitic magmas in 3–5-Ma-old crust. In the area of Easter Island, the crust has an age of ~4 Ma but the crust is probably thickened owing to the intraplate magmatism and the hotspot influence on the ridge

(Woods & Okal, 1994). Because plagioclase appears to follow olivine on the liquidus of the submarine basalts (e.g. 35DS and 36DS samples) the crystallization probably occurs at levels shallower than 0·7 GPa (Presnall *et al.*, 1979; Grove *et al.*, 1992), implying a magma reservoir at <20 km depth. Magmas may fractionate in this reservoir until they reach an *mg*-number between 65 and 55 (the density minimum for tholeiitic liquids; Stolper & Walker, 1980), after which they ascend and erupt. The submarine basalts have *mg*-numbers in this range, whereas the subaerial lavas generally have *mg*-numbers <50, indicating that they may have another, shallower compensation and stagnation level as discussed above. The decrease of melt production in the mantle beneath the volcano as the plate transports it away from the plume centre probably also leads to a stagnation of ascending melts at shallow levels (e.g. Frey *et al.*, 1990).

A model for the partial melting of the mantle source of the magmas

Constraints on primary magmas and mantle sources

Most of the differences in incompatible element contents and $(La/Sm)_N$ ratios between the three groups of lavas of the Easter Hotspot probably arose either during partial melting processes in the mantle or are due to the generation of the magmas from mantle sources of different compositions. In Fig. 8a we show a plot of $^{143}Nd/^{144}Nd$ vs $^{87}Sr/^{86}Sr$ isotopes of the Easter Hotspot lavas. Most have higher $^{87}Sr/^{86}Sr$ and lower $^{143}Nd/^{144}Nd$ isotope ratios than MORB from the East Pacific Rise and the Easter Microplate. With the exception of two Volcanic Fields Group lavas and two Main Group lavas the Easter Hotspot samples are isotopically distinct from the enriched tholeiites from the Ahu and Umu volcanic fields closer to the spreading axis (Fig. 8a). The variation in the Sr–Nd isotope compositions can be explained by mixing of material from an enriched plume and a depleted MORB source (Haase *et al.*, 1996). The same can be observed in Fig. 8b,where most lavas from Easter Island and the seamounts plot outside the fields of MORB and the enriched Ahu and Umu Volcanic Fields tholeiites but there is an overlap. The most enriched lavas (the Roiho group) have the highest $(La/Sm)_N$ and lowest $^{143}Nd/^{144}Nd$ but there are several Main Group and Volcanic Fields Group samples with low $^{143}Nd/^{144}Nd$ and high $(La/Sm)_N$ (Fig. 8b). The different Sr–Nd isotope compositions of the samples imply time-integrated variations of the Sm/Nd and Rb/Sr in their sources. However, the occurrence of lavas with similar isotopic signatures but very different $(La/Sm)_N$ suggests a recent fractionation of the incompatible elements owing to partial melting. Thus, it appears that several magmas with highly variable $(La/Sm)_N$ were generated from one source containing similar amounts of enriched plume and depleted MORB end-member material. In the following, we will present a model for the partial melting process.

Most of the Easter Hotspot lavas have MgO contents which are too low, and olivine phenocrysts which are too fayalitic (Fo <85%) for them to be primitive mantle melts (Fig. 3). However, in each of the groups one of the most mafic samples (MgO 7·8–8·7%) was selected for the modelling of the melting history (43DS-1gl, 27DS-2gl and 43DS-2 for the Volcanic Fields, Main Group and Roiho Group, respectively). None of the selected samples contains clinopyroxene phenocrysts and only small amounts of plagioclase were observed so that we assume that the samples did not fractionate significant amounts of this phase. The MgO content of the primary magmas is unknown and no extremely forsteritic olivines were found (Fig. 3), which might indicate a possible primary magma in equilibrium with mantle olivine (>Fo_{88}, Frey *et al.*, 1978). Thus we added olivine of composition Fo_{87} to the three selected samples, giving contents of ~12% MgO for 10% and ~15·5% MgO for 20% of added olivine in the magma. The MgO contents of these calculated liquids equal *mg*-numbers of 67·7–71·0 and 73·2–75·1, respectively, which would be in equilibrium with mantle olivine $Fo_{89–91}$ assuming a $K_d^{Ol–Liq}$ of 0·3 (Roeder & Emslie, 1970) and $FeO = FeO^T \times 0{\cdot}86$. The three selected lavas have comparable Nd isotopic compositions but their Sr isotope compositions differ, suggesting a heterogeneous source. However, as we have discussed above, the variable $(La/Sm)_N$ ratios could be the result of the partial melting processes rather than different source compositions. In an approach to determine the degree of melting of the source of the Easter Hotspot magmas, we will discuss the major element compositions and compare them with results of recent experiments.

The degree of partial melting inferred from the major element chemistry of the magmas

Experimental petrology generally suggests that alkali basalts comparable in composition with the Roiho Group lavas form by an average degree of partial melting of 3–10% whereas tholeiites like 43DS-1 are probably due to higher degrees of melting at >8% (Jaques & Green, 1980; Takahashi & Kushiro, 1983). On the basis of an REE melting model, Haase & Devey (1996) have shown that the Ahu Volcanic Field tholeiites formed by 8–10% partial melting at higher average pressures than that at which MORB on the neighbouring spreading axis is generated. The lavas of Easter Island and the seamounts erupted on older lithosphere than the Volcanic Fields magmas, and, according to the model of Haase & Devey (1996), formed at higher pressures and lower degrees of

melting because their melting column was shorter because of the thicker lithosphere. Here we will test this model further using recently published experiments on the partial melting of mantle peridotite in which the degrees of melting were determined (Hirose & Kushiro, 1993; Baker & Stolper, 1994; Kushiro, 1996). On the basis of these experiments we chose Na_2O and the ratio of CaO/Al_2O_3 to determine the degree of melting because these two parameters should reflect mainly the amount of clinopyroxene dissolved in the melt. Although there is a pressure dependence because of the changing compatibility of Na in clinopyroxene (Blundy *et al.*, 1995) and of Al in the Al phases present, the trends in Fig. 10a and b suggest that the pressure influence is of minor importance relative to the degree of melting. The experiments are limited to degrees of melting >2%, owing to the techniques used. All experiments agree that Na_2O decreases whereas the CaO/Al_2O_3 value increases with increasing degree of partial melting. To compare the trends of each experimental study with our possible primary magmas, logarithmic least-squares curves were fitted to the experimental results. Variations in the curves are probably due to the different compositions of the source peridotites used in the different studies. Two Na_2O values at low degrees of melting from the Hirose & Kushiro (1993) experiments were omitted because these values were apparently too high compared with those for higher degrees of melting and the other two experimental studies. Using the curves calculated in Fig. 10a and 10b we construct a melting 'grid' for the two parameters in Fig. 10c and plot the three selected most primitive mafic lavas as well as their compositions with added olivine. The source compositions used in the experiments range from slightly depleted peridotites (KLB-1 and PHN) to primitive mantle (PRIMA), and thus probably cover the source composition range of the Easter Hotspot magmas as there is no evidence for a strongly enriched source nor a very depleted one. The slopes of the curves calculated for the Baker & Stolper (1994) and the Kushiro (1996) experiments agree but show that Na_2O may depend strongly on the composition of the peridotite source. The curve from the experiments of Hirose & Kushiro (1993) is slightly flatter than the other two. As we pointed out above, none of the primitive Easter Hotspot magmas contains clinopyroxene phenocrysts, which could change the CaO/Al_2O_3 ratio significantly. With the addition of 10% olivine (i.e. assumed primary magmas with ~12% MgO), the three selected magmas lie on the curve of the Baker & Stolper (1994) experiments. Although the uncertainties are large, as a result of the unknown source compositions, compositions of the true primary magmas and pressures of melting, the Baker & Stolper (1994) and the Kushiro (1996) experiments both suggest degrees of melting between ~8% for the Roiho Group magma and 10 or 12% for the Volcanic Fields Group lava. These results are within the range suggested by Haase & Devey (1996), and because of the close agreement of the two experimental data sets we prefer them to the Hirose & Kushiro (1993) curve, which gives higher degrees of melting between 11 and 16%. We believe that our approach gives relatively robust results, although melting probably is dynamic and the erupting magma is a mixture of melts from a large melting column. In particular, the incompatible element Na might be influenced by small-degree melts from deep in the column. However, the actual degrees of melting we obtain for a given composition are comparable with those of dynamic melting models similar to that of Langmuir *et al.* (1992).

The degree of melting based on rare earth elements

The REE contents of the lavas reflect the degree of partial melting, but also depend on the source composition. Using a depleted MORB source for the Easter Hotspot magmas would imply very low degrees of partial melting to account for the strong LREE enrichment in many Easter Hotspot lavas, which we believe to be unlikely for two reasons: (1) the Sr–Nd isotope data suggest that the mantle source is more enriched than the MORB source (Fig. 8a, Macdougall & Lugmair, 1986; Haase *et al.*, 1996); (2) according to currently available experimental data, the major elements indicate relatively large degrees of melting (Fig. 10). Nevertheless, the Nd isotope composition of the Easter Hotspot lavas implies a time-integrated Nd/Sm depletion compared with Bulk Earth. The fractionation of the HREE observed in the lavas indicates the presence of residual garnet in the mantle (e.g. Kay *et al.*, 1970). Figure 11a shows a model for REE in which the mantle begins to melt at depths where garnet peridotite is stable and the main melting takes place in the spinel peridotite stability field. In the model, melts from 1% melting steps are accumulated and the composition of the mantle is recalculated after each step with respect to residual minerals and element concentrations. A slightly LREE-enriched plume source was assumed that is capable of producing both the observed variation of the LREE in the mafic magmas as well as the Sr–Nd isotopic compositions observed (Haase & Goldstein, in preparation). The composition of the mafic magmas with 10% added olivine is shown because the primary Easter Hotspot magmas probably had MgO contents not higher than 12%, resulting in *mg*-numbers of 68–71, i.e. approximately the range of primary magmas (e.g. Frey *et al.*, 1978). The modelled REE fit the patterns of the three assumed primary magmas and the increasing degrees of melting from the Roiho to the Volcanic Fields Group are qualitatively in accordance with the major element model. However, the quantitative results of the REE model are lower than those of the major element models for the most enriched basalt, which is modelled

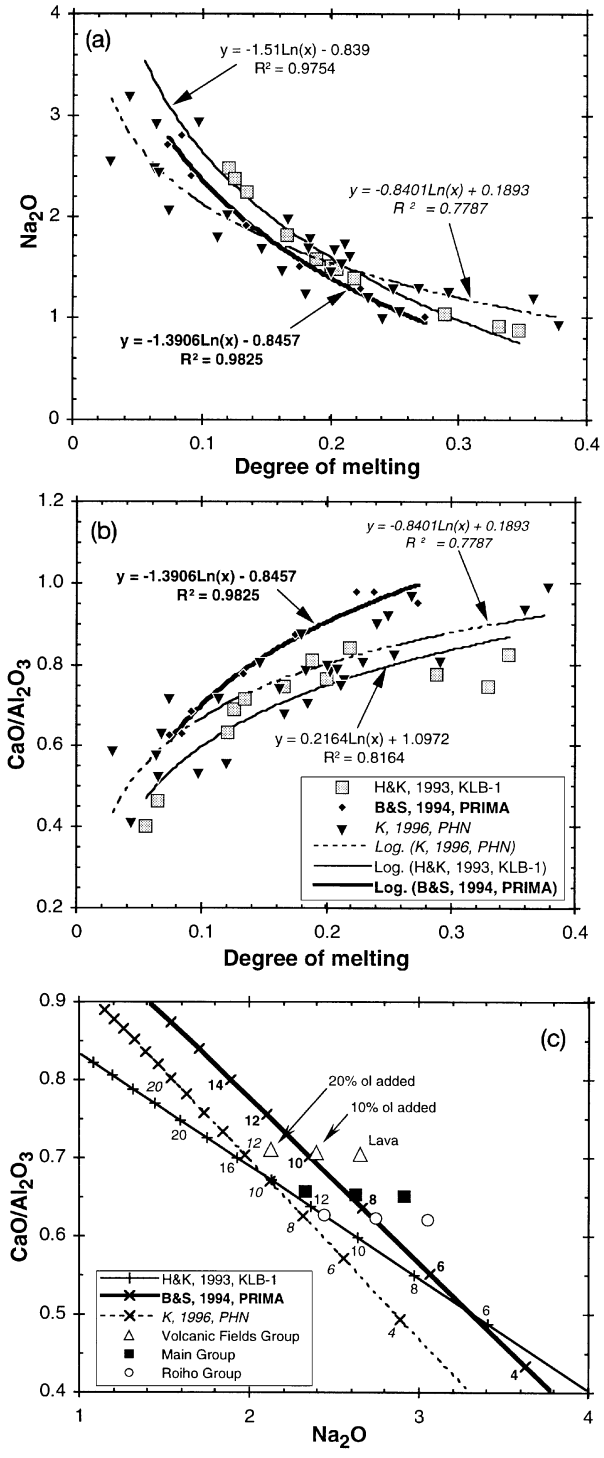

by ~5% melting compared with ~8% in the major element model (Fig. 11a). On the other hand, the more depleted magmas give consistent degrees of melting of ~10% in both models. The Sr–Nd isotope data suggest that the source of the more depleted magmas contains considerably more MORB mantle (~60%, Haase *et al.*, 1996) than the 'pure' inferred plume source, leading to a decrease of the degree of melting. This is shown in Fig. 11b, where the enriched source is mixed with 60% MORB mantle and an 8% melt from this source accounts for the REE composition of the enriched Volcanic Fields tholeiite group. The most enriched magma could have formed from ~3% melting from such a source (Fig. 11b) but our preferred model is that these magmas are derived from a more enriched source resembling the one shown in Fig. 11a. Further experimental data for low-degree partial melts are required to provide insights into the possible decoupling of elements owing to different compatibility to the mantle source. The high concentrations of the incompatible elements in the most enriched magmas may be due to the sampling of a larger volume of source mantle by incompatible element enriched small-degree melts which then mix with large-degree melts (Galer & O'Nions, 1986). Three-dimensional REE melting models for Hawaii gave higher concentrations for larger degrees of melting because of larger contributions from low-degree melts (Eggins, 1992). However, to explain the whole range of observed Hawaiian magmas an enriched source was required (Eggins, 1992), and fluid dynamic studies suggest that small-degree melts from the plume margin do not flow towards the plume centre (Ribe & Smooke, 1987). Nevertheless, our major element and REE models for the Easter Hotspot data indicate that the degree of partial melting decreases significantly from the tholeiites to the alkaline lavas and that the alkaline magmas are probably dominated by melts formed at greater pressures and from more enriched sources. This suggests that the melting processes in the Easter Hotspot are highly variable although the total life span of the volcanoes appears to be very short (<1 Ma).

The chemical evolution of the Easter Hotspot

A temporal chemical evolution of volcanoes has been observed on oceanic islands such as Hawaii (Clague &

Fig. 10. (a) Na_2O contents of experimentally derived partial melts of peridotite plotted vs degree of partial melting. The melts are from two slightly depleted peridotites (KLB-1 and PHN1611) and one with the inferred composition of primitive mantle (PRIMA) (Hirose & Kushiro, 1993; Baker & Stolper, 1994; Kushiro, 1996). The curves are least-squares fits to the experimental data and the equations of each curve are given. (b) Similar plot to (a) for CaO/Al_2O_3. (c) CaO/Al_2O_3 vs Na_2O for three mafic Easter Hotspot lavas representing the three groups. These lavas do not show signs of clinopyroxene fractionation. The effect of addition of 10% and 20% olivine with Fo_{87} is shown by the symbols at lower Na_2O. Also shown are lines of variable degrees of partial melting (indicated by tick marks with numbers in per cent) derived from the curves and the experiments in (a) and (b).

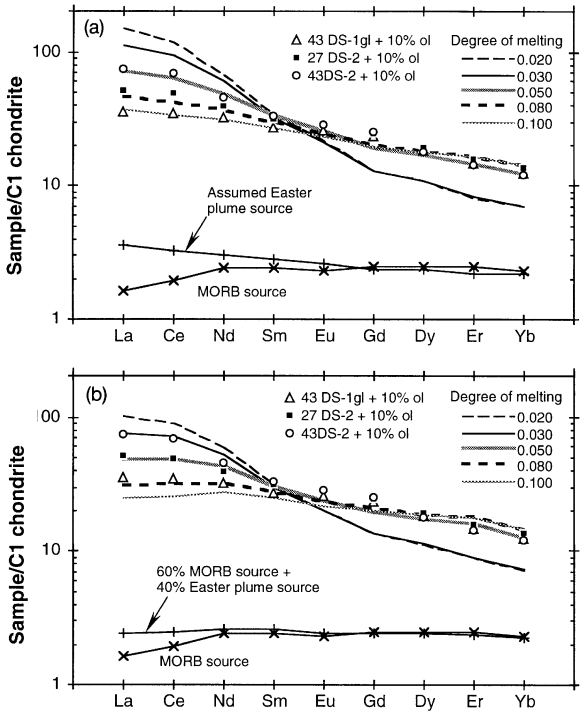

Fig. 11. (a) C1 chondrite-normalized REE diagram showing the three assumed parent magmas of each lava group (43DS-2, 43DS-1gl and 27DS-2gl) with 10% olivine added. Different curves for modelled accumulated Rayleigh melts are shown with the numbers indicating the degrees of melting. The melts are products of accumulated melting in 1% steps, the first 3% occurring in the garnet peridotite field after which melting takes place in the spinel peridotite stability field. We used the compilation of distribution coefficients by Kelemen *et al.* (1993) and the modal mineralogy in the garnet stability fields D (60% ol + 20% opx + 14% cpx + 6% gar) and P (55% cpx + 40% gar + 1% ol + 4% opx). In the spinel stability field D changes to 61·2% ol + 20·3% opx + 13·5% cpx + 2·5% sp and P to 75% cpx + 15% sp + 2% ol + 8% opx. The chondrite normalizing compositions are taken from Sun & McDonough (1989) and the depleted MORB source was calculated by dividing the average of Hofmann (1988) by the factor ten. (b) Same as (a) but calculated for a mixed source containing 40% enriched plume and 60% MORB source material.

Dalrymple, 1987) and also for near-ridge seamounts (Batiza & Vanko, 1984) where the major shield-building stages are tholeiitic and late low-volume stages are alkaline. Thus, it might be expected that the compositional variations between the lava suites of the Easter Hotspot are also time dependent. Relatively incompatible element depleted lavas comparable with those of the young volcanic fields on ~2 Ma old crust (Fig. 1) occur on the submarine pedestal of Easter Island (Rano Kau Ridge, 24DS) and on the seamounts. Their restriction to the submarine part of the volcanoes possibly suggests that the early submarine stage of volcanism at the Easter Hotspot formed by larger degrees of melting and was more strongly influenced by MORB source material (Haase & Devey, 1996; Haase *et al.*, 1996), owing to the position of the volcanoes closer to the spreading axis of the East Rift. The ages (O'Connor *et al.*, 1995) of three samples from Easter Island and the seamounts (situated on 3–4 Ma old crust) support this model, as the Volcanic Fields lava from Pukao Seamount (35DS-1a) is the oldest whereas the Roiho Group lava gives the youngest age (Fig. 6). Assuming a spreading rate of ~100 km/Ma (Naar & Hey, 1991) this lava would have formed in the region of the present Ahu and Umu Volcanic Fields (Fig. 1a). The more enriched Main Group lavas of the island and the seamounts formed within 0·7 Ma on crust of the age of that underlying Pukao Seamount at present (Fig. 1a). Tholeiitic rocks were recovered at greater water depths and they appear to be restricted to depths >1000 m. The two more enriched lava groups were found over the whole depth range, possibly suggesting that the more enriched lavas form cappings on the older edifices but also form small cones scattered on the seafloor or on the flanks of larger edifices. By analogy to the Hawaiian and off-axis East Pacific Rise volcanoes (e.g. Seamount 6, Batiza & Vanko, 1984), we suggest that a relatively incompatible element depleted tholeiitic phase, which is now observed, for example, on the Ahu Volcanic Field, forms above the plume in proximity to the spreading axis. The volcano drifts away from the plume region closest to the spreading axis and when the lithosphere underneath the volcano reaches an age of ~3 Ma as at present at Pukao Seamount, more alkaline lavas form. Similarly, Batiza & Vanko (1984) observed that off-axis seamount lavas erupting on crust younger than 3 Ma are generally uniformly depleted whereas lavas on older crust are more variable and often alkaline. Thus we will compare the chemical variation observed at known multi-stage volcanoes with the situation at the Easter Hotspot.

Figure 12 shows a plot of Nb/Zr vs $(La/Sm)_N$ for the Easter Hotspot lavas compared with submarine and subaerial volcanics from Mauna Kea on Hawaii. Whereas the enriched tholeiites from the volcanic fields, the seamounts and Rano Kau Ridge resemble the shield tholeiites of Mauna Kea, the more alkaline Main Group and the Roiho Group basalts fall into two distinct groups, lying on and to the enriched end of the field for the Mauna Kea postshield alkali basalts. Recent drilling studies on Mauna Kea found flow-to-flow variations implying complex variations in the partial melting processes (e.g. Yang *et al.*, 1996). However, these short-term variations, for instance, within the tholeiitic part of the section are small (Nb/Zr 0·07–0·1, Yang *et al.*, 1996) compared with the long-term variations observed in Hawaii and the Easter Hotspot (Fig. 12a). Although the flow-to-flow variations suggest short-term changes in the degree of partial melting in plumes they do not change the long-term pattern of volcano evolution through different magmatic stages. The Easter Hotspot lavas do not show the significant isotopic differences between the stages that occur in the Hawaii and East Pacific Rise off-axis

Seamount 6 basalts (e.g. Zindler *et al.*, 1984; Chen & Frey, 1985; Frey *et al.*, 1990). On the other hand, as in the Seamount 6 case, the most incompatible element enriched lavas from the Easter Hotspot have the highest $^{87}Sr/^{86}Sr$ whereas the enriched Volcanic Fields tholeiites and comparable lavas from the seamounts generally have lower $^{87}Sr/^{86}Sr$ ratios (Fig. 8). The overlap in the isotopic compositions between incompatible enriched and depleted lavas probably implies variable mixing between the MORB source and the plume end-members as well as variable degrees of melting. In Fig. 12b we compare the relative enrichment in incompatible element ratios Ta/Hf vs $(La/Sm)_N$ in lavas from the Easter Hotspot and the off-ridge Seamount 6. Batiza (1980) suggested a transition from the eruption of MORB-like tholeiites to alkali basalts with time for non-plume near-ridge seamounts in response to increasing lithospheric age. The lavas from the well-studied Seamount 6 form three groups, two of which are tholeiitic and consist of MORB-like depleted tholeiites trending to enriched tholeiites (Fig. 12b). Alkaline basalts form late-stage cappings on Seamount 6 and have relatively low MgO contents like the relatively alkaline Easter Hotspot lavas but are more enriched in incompatible elements. The enriched Volcanic Fields tholeiite group from the Easter Hotspot show a similar incompatible element enrichment to the tholeiites from the Mauna Kea shield phase and Seamount 6. This similar variation of the Easter Hotspot lavas supports our suggestion that the volcanism develops through an early tholeiitic submarine stage followed by the more alkaline volcanism capping the seamounts and Easter Island. Whereas Seamount 6 shows the compositional transition on one volcano over <5 Ma, we may observe this transition contemporaneously in the volcanoes of the Easter Hotspot resting on lithosphere of various ages.

Clearly, more age data on the Easter Hotspot volcanism are required to confirm the evolution of this near-ridge hotspot. Also, the seamounts east of Easter Island along the Sala y Gomez Ridge have to be sampled in more detail to investigate whether they evolved through several chemically distinct stages. Most of the data available at present suggest that only alkaline lavas were sampled with $(La/Sm)_N$ of 1·7–2·7 (Bonatti *et al.*, 1977). However, a Nd isotope ratio of 0·51302 for the altered basalt GS7202-96 (Cheng, 1989) falls into the range of the tholeiitic stage of the Easter Hotspot volcanism (Fig. 8a), possibly implying the occurrence of more depleted rocks along the plume track. Unfortunately, further chemical data for this sample are not available. Given the scarcity of data and the shallow recovery of the samples from the Sala y Gomez Ridge (except one all are <2000 m; Bonatti *et al.*, 1977) it appears likely that only the alkaline capping volcanics were sampled.

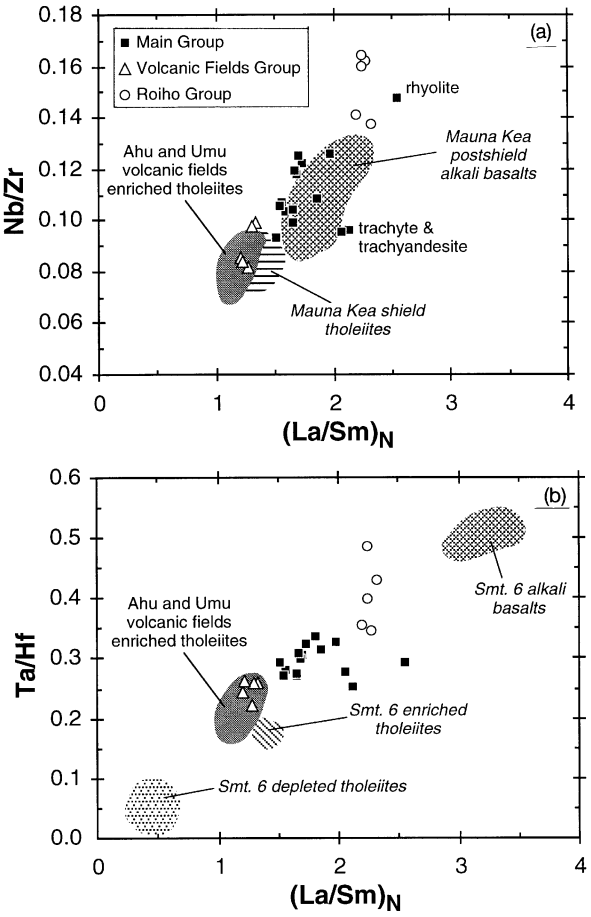

Fig. 12. (a) A comparison of Nb/Zr vs $(La/Sm)_N$ of the Easter Hotspot lavas with the two submarine and subaerial stages observed at Mauna Kea, Hawaii; (b) a comparison of Ta/Hf vs $(La/Sm)_N$ for the Easter lavas with the three stages observed at Seamount 6 at 20°N near the East Pacific Rise. Also included are fields for enriched tholeiites from the young volcanic fields 150 km west of Easter Island from Haase & Devey (1996) and Fretzdorff *et al.* (1996). Data are from Batiza & Vanko (1984), Frey *et al.* (1990) and Yang *et al.* (1994).

CONCLUSIONS

Lavas from Easter Island and the two neighbouring seamounts Moai and Pukao can be grouped into three lava series based on their $(La/Sm)_N$ ratios. The samples with $(La/Sm)_N$ of ~1·2 are tholeiitic and comparable with the most abundant lavas found on the young volcanic fields 150 km west of Easter Island. The other two groups are transitional to alkaline, one having an intermediate enrichment of $(La/Sm)_N$ 1·5–2 whereas several basalts are even more enriched [$(La/Sm)_N$ ~2·3]. Within each of the three lava groups the members are probably related by crystal fractionation but only the Main Group of transitional tholeiites shows extensive fractionation, ranging from basalts to rhyolite and trachyte on Easter Island. This suggests that a shallow magma chamber formed underneath Easter Island but not underneath the

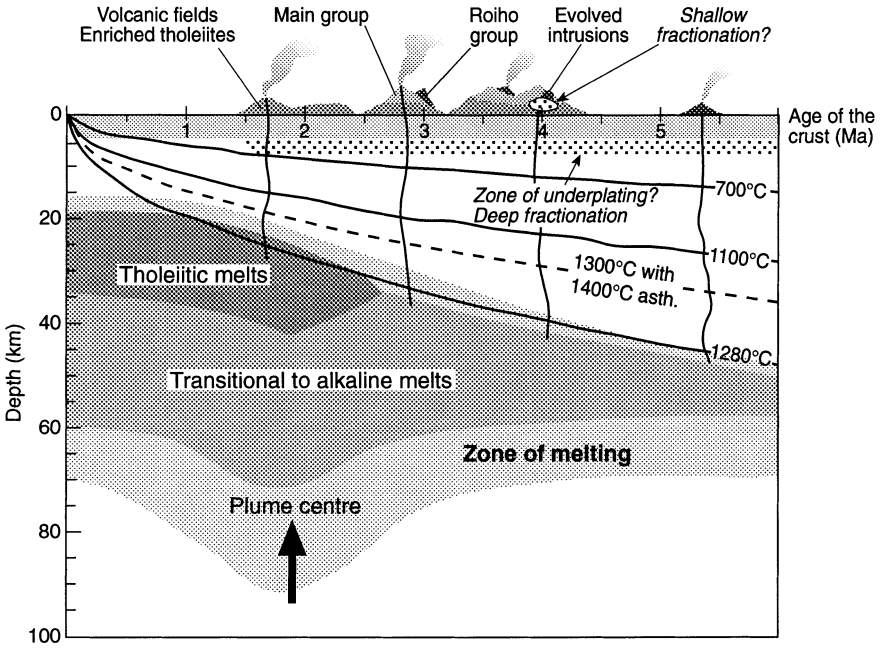

Fig. 13. Schematic model for the petrogenetic evolution of the Easter Hotspot magmas. The isotherms were calculated according to Parsons & Sclater (1977) and the broken line is for the case of the plume warming the asthenosphere to 1400°C, i.e. thinning the lithosphere. (See the text for discussion.)

submarine volcanoes because the lavas recovered there are only slightly fractionated. The presence of large phenocrysts and xenocrysts in many submarine lavas implies the stagnation of the ascending magmas in larger reservoirs possibly at lower-crustal levels. From the available ages and the depth range over which the lavas occur we suggest two or three stages of magmatism occurring at the Easter Hotspot. The possible evolution of this near-ridge hotspot is shown schematically in Fig. 13. An early tholeiitic stage forms large volcanoes at depths >1000 m below sea-level. These magmas are generated when the volcano is close to the spreading axis and thus contains a large MORB source component with the thin lithosphere allowing relatively large degrees of partial melting. This stage is succeeded by the transitional Main Group stage, which can be observed subaerially on Easter Island and forms the cappings of the seamounts. A third series consisting of the most enriched Roiho Group lavas appears to form small centres of eruption on volcanoes or as flank cones on the seafloor (Fig. 13). The degree of partial melting decreases from ~10% for the tholeiitic to perhaps 5–8% for the most enriched basalt group. As the lithosphere becomes thicker with age, the zone of partial melting is depressed to greater depths, leading to an increased average pressure of melting for each of the three stages. At the same time, the influence of the MORB source material flowing in from the spreading axis decreases and thus the magmas generally contain a greater amount of the more enriched plume component. The decreasing magma supply to the large volcanic edifices leads to the solidification of a shallow magma chamber in which strongly evolved magmas can form. These eventually rise to form late eruptive centres and late-stage plugs in the large volcanoes (Fig. 13). Depending on the volume and composition of fractionating phases, the evolved magmas may consist of either rhyolites (Rano Kau) or trachytes (Poike). The rhyolites fractionated significantly larger volumes of plagioclase and K-feldspar than the trachytes, possibly owing to lower pressure and water contents during the genesis of the former.

The similarities of the fractionation trends and the abundance of variably enriched lava suites at other near-ridge hotspots such as the Galapagos and on Iceland suggest comparable evolutionary histories for these magmatic systems. However, because these hotspots have more complicated tectonic situations influencing their magmatic evolution, the trends observed may be less systematic. For instance, the lithospheric thickness beneath the Galapagos volcanoes varies not only normal to the spreading axis but also laterally, and some of the volcanoes closest to the spreading axis (Darwin, Wolf) lie on a fracture zone cutting through the archipelago (e.g. Feighner & Richards, 1994). Thus the Easter Hotspot may provide the simplest and most representative case study of near-ridge hotspot evolution.

ACKNOWLEDGEMENTS

We thank Captain Kull and his crew of FS *Sonne* for their help during the cruise. D. Ackermand and B. Mader are thanked for their help with the electron microprobe, and T. Arpe for help with the inductively coupled plasma mass spectrometer. We appreciate discussions and comments by C. Devey, S. Goldstein, A. Hofmann and J. O'Connor on earlier versions of this manuscript. We thank the official reviewers P. E. Baker, M. O. Garcia and D. J. Geist and the editor M. Wilson, whose comments significantly improved the quality of the paper. K.M.H. gratefully acknowledges financial support by the Deutsche Forschungsgemeinschaft. This study was made possible through BMBF Grant STO03R420A to P. Stoffers.

REFERENCES

Abers, G. A., Parsons, B. & Weissel, J. K., 1988. Seamount abundances and distribution in the southeast Pacific. *Earth and Planetary Science Letters* **87,** 137–151.

Bach, W., Hegner, E., Erzinger, J. & Satir, M., 1994. Chemical and isotopic variations along the superfast spreading East Pacific Rise from 6 to 30°S. *Contributions to Mineralogy and Petrology* **116,** 365–380.

Baitis, H. W. & Lindstrom, M. M., 1980. Geology, petrography, and petrology of Pinzon Island, Galapagos Archipelago. *Contributions to Mineralogy and Petrology* **72,** 367–386.

Baker, M. B. & Stolper, E. M., 1994. Determining the composition of high-pressure mantle melts using diamond aggregates. *Geochimica et Cosmochimica Acta* **58,** 2811–2827.

Baker, P. E., 1973. Islands in the South Atlantic. In: Nairn, A. E. H. & Stehli, F. G. (eds) *The Ocean Basins and Margins; Vol. 1, The South Atlantic*. New York: Plenum, pp. 493–553.

Baker, P. E., Buckley, F. & Holland, J. G., 1974. Petrology and geochemistry of Easter Island. *Contributions to Mineralogy and Petrology* **44,** 85–100.

Batiza, R., 1980. Origin and petrology of young oceanic central volcanoes: Are most tholeiitic rather than alkalic? *Geology* **8,** 477–482.

Batiza, R. & Vanko, D., 1984. Petrology of young Pacific seamounts. *Journal of Geophysical Research* **89,** 11235–11260.

Blundy, J. D., Falloon, T. J., Wood, B. J. & Dalton, J. A., 1995. Sodium partitioning between clinopyroxene and silicate melts. *Journal of Geophysical Research* **100,** 15501–15515.

Bonatti, E., Harrison, C. G. A., Fisher, D. E., Honnorez, J., Schilling, J.-G., Stipp, J. J. & Zentilli, M., 1977. Easter volcanic chain (Southeast Pacific): a mantle hot line. *Journal of Geophysical Research* **82,** 2457–2478.

Chen, C.-Y. & Frey, F. A., 1985. Trace element and isotopic geochemistry of lavas from Haleakala volcano, East Maui, Hawaii: implications for the origin of Hawaiian basalts. *Journal of Geophysical Research* **90,** 8743–8768.

Cheng, Q. C., 1989. Geochemical studies of hotspot volcanism in the southern Pacific and its implications for mantle structure and dynamics. Ph.D. Thesis, University of California, San Diego.

Clague, D. A. & Dalrymple, G. B., 1987. The Hawaiian–Emperor volcanic chain, Part I, Geologic evolution. *US Geological Survey Professional Paper* **1350,** 5–54.

Clague, D. A., Weber, W. S. & Dixon, J. E., 1991. Picritic glasses from Hawaii. *Nature* **353,** 553–556.

Clark, J. G. & Dymond, J., 1977. Geochronology and petrochemistry of Easter and Sala y Gomez Islands: implications for the origin of the Sala y Gomez Ridge. *Journal of Volcanology and Geothermal Research* **2,** 29–48.

Condomines, M., Grönvold, K., Hooker, P. J., Muehlenbachs, K., O'Nions, R. K., Oskarsson, N. & Oxburgh, E. R., 1983. Helium, oxygen, strontium and neodymium isotopic relationships in Icelandic volcanics. *Earth and Planetary Science Letters* **66,** 125–136.

Cullen, A. & McBirney, A. R., 1987. The volcanic geology and petrology of Isla Pinta, Galapagos archipelago. *Geological Society of America Bulletin* **98,** 294–301.

Eggins, S. M., 1992. Petrogenesis of Hawaiian tholeiites: 2, aspects of dynamic melt segregation. *Contributions to Mineralogy and Petrology* **110,** 398–410.

Ellam, R. M., 1992. Lithospheric thickness as a control on basalt geochemistry. *Geology* **20,** 153–156.

Feigenson, M. D., Hofmann, A. W. & Spera, F. J., 1983. Case studies on the origin of basalt II. The transition from tholeiitic to alkalic volcanism on Kohala volcano, Hawaii. *Contributions to Mineralogy and Petrology* **84,** 390–405.

Feighner, M. A. & Richards, M. A., 1994. Lithospheric structure and compensation mechanisms of the Galapagos Archipelago. *Journal of Geophysical Research* **99,** 6711–6729.

Fretzdorff, S., Haase, K. H. & Garbe-Schönberg, C.-D., 1996. Petrogenesis of lavas from the Umu Volcanic Field in the young hotspot region west of Easter Island, southeastern Pacific. *Lithos* **38,** 23–40.

Frey, F. A., Green, D. H. & Roy, S. D., 1978. Integrated models of basalt petrogenesis: a study of quartz tholeiites to olivine melilitites from south eastern Australia utilizing geochemical and experimental petrological data. *Journal of Petrology* **19,** 463–513.

Frey, F. A., Garcia, M. O., Wise, W. S., Kennedy, A., Gurriet, P. & Albarède, F., 1990. The evolution of Mauna Kea volcano, Hawaii: petrogenesis of tholeiitic and alkalic basalts. *Journal of Geophysical Research* **96,** 14347–14375.

Furman, T., Frey, F. A. & Meyer, P. S., 1992. Petrogenesis of evolved basalts and rhyolites at Austurhorn, Southeastern Iceland: the role of fractional crystallization. *Journal of Petrology* **33,** 1405–1445.

Galer, S. J. G. & O'Nions, R. K., 1986. Magmagenesis and the mapping of chemical and isotopic variations in the mantle. *Chemical Geology* **56,** 45–61.

Garbe-Schönberg, C.-D., 1993. Simultaneous determination of 37 trace elements in 28 international rock standards by ICP-MS. *Geostandards Newsletters* **17,** 81–97.

Geist, D. J., Baker, B. H. & McBirney, A. R., 1985. GPP, a program package for creating and using geochemical data files. Eugene: University of Oregon.

Geist, D., Howard, K. A. & Larson, P., 1995. The generation of oceanic rhyolites by crystal fractionation: the basalt–rhyolite association at Volcán Alcedo, Galápagos Archipelago. *Journal of Petrology* **36,** 965–982.

Gonzalez-Ferran, O., Carmona, R. & Katsui, Y., 1968. Mapa geologico Isla de Pascua, 1:5000. Instituto Geografico Militar de Chile.

Gonzalez-Ferran, O., Cordani, U. G. & Halpern, M., 1974. Potassium–argon ages and $^{87}Sr/^{86}Sr$ ratios of volcanic rocks from Easter Island. *Proceedings of the Symposium on Andean and Antarctic Volcanology Problems*. Santiago, Chile: International Association of Volcanology and Chemistry of the Earth's Interior, pp. 1–10.

Grove, T. L., Kinzler, R. J. & Bryan, W. B., 1992. Fractionation of mid-ocean ridge basalt (MORB). In: Phipps Morgan, J., Blackman, D. K. & Sinton, J. M. (eds) *Mantle Flow and Melt Generation at Mid-ocean Ridges. Geophysical Monograph, American Geophysical Union* **71,** 281–310.

Haase, K. M., 1995. Magmagenesis in a plume–ridge system: the Easter Hotspot–Easter Microplate case, SE Pacific. Ph.D. Thesis, University of Kiel, 120 pp.

Haase, K. M., 1996. The relationship between the age of the lithosphere and the composition of oceanic magmas: constraints on partial melting, mantle sources and the thermal structure of the plates. *Earth and Planetary Science Letters* **144,** 75–92.

Haase, K. M. & Devey, C. W., 1996. Geochemistry of lavas from the Ahu and Tupa volcanic fields, Easter Hotspot, SE Pacific: implications for intraplate magma genesis near a spreading axis. *Earth and Planetary Science Letters* **137,** 129–143.

Haase, K. M., Devey, C. W. & Goldstein, S. L., 1996. Two-way exchange between the Easter mantle plume and the Easter Microplate spreading axis. *Nature* **382,** 344–346.

Hagen, R. A., Baker, N. A., Naar, D. F. & Hey, R. N., 1990. A SeaMARC II survey of recent submarine volcanism near Easter Island. *Marine Geophysical Researches* **12,** 297–315.

Hanan, B. B. & Schilling, J.-G., 1989. Easter Microplate evolution: Pb evidence. *Journal of Geophysical Research* **94,** 7432–7448.

Harland, W. B., Armstrong, R. L., Cox, A. V., Craig, L. E., Smith, A. G. & Smith, D. G., 1990. *A Geologic Time Scale 1989*. Cambridge: Cambridge University Press, 263 pp.

Harris, C., 1983. The petrology of lavas and associated plutonic inclusions of Ascension Island. *Journal of Petrology* **24,** 424–470.

Hart, S. R. & Brooks, C., 1974. Clinopyroxene–matrix partitioning of K, Rb, Cs, Sr and Ba. *Geochimica et Cosmochimica Acta* **38,** 1799–1806.

Hart, S. R. & Staudigel, H., 1989. Isotopic characterization and identification of recycled components. In: Hart, S. R. & Gülen, L. (eds) *Crust/Mantle Recycling at Convergence Zones*. Dordrecht: Kluwer Academic, pp. 15–28.

Hirose, K. & Kushiro, I., 1993. Partial melting of dry peridotites at high pressures: determination of compositions of melts segregated from peridotite using aggregates of diamond. *Earth and Planetary Science Letters* **114,** 477–489.

Hofmann, A. W., 1988. Chemical differentiation of the Earth: the relationship between mantle, continental crust, and oceanic crust. *Earth and Planetary Science Letters* **90,** 297–314.

Holloway, J. R. & Burnham, C. W., 1972. Melting relations of basalt with equilibrium water pressure less than total pressure. *Journal of Petrology* **13,** 1–29.

Imsland, P., Larsen, J. G., Prestvik, T. & Sigmond, E. M., 1977. The geology and petrology of Bouvetøya, South Atlantic Ocean. *Lithos* **10,** 213–234.

Isaacson, L. B. & Heinrichs, D. F., 1976. Paleomagnetism and secular variation of Easter Island basalts. *Journal of Geophysical Research* **81,** 1476–1482.

Jaques, A. L. & Green, D. H., 1980. Anhydrous melting of peridotite at 0–15 kbar pressure and the genesis of tholeiitic basalts. *Contributions to Mineralogy and Petrology* **73,** 287–310.

Kaneoka, I. & Katsui, Y., 1985. K–Ar ages of volcanic rocks from Easter Island. *Bulletin of the Volcanological Society of Japan* **30,** 33–36.

Kay, R., Hubbard, N. J. & Gast, P. W., 1970. Chemical characteristics and origin of oceanic ridge volcanic rocks. *Journal of Geophysical Research* **75,** 1585–1613.

Kelemen, P. B., Shimizu, N. & Dunn, T., 1993. Relative depletion of niobium in some arc magmas and the continental crust: partitioning of K, Nb, La and Ce during melt/rock reaction in the upper mantle. *Earth and Planetary Science Letters* **120,** 111–134.

Kushiro, I., 1980. Viscosity, density, and structure of silicate melts at high pressures, and their petrological applications. In: Hargraves, R. B. (ed.) *Physics of Magmatic Processes*. Princeton, NJ: Princeton University Press, pp. 93–120.

Kushiro, I., 1996. Partial melting of a fertile mantle peridotite at high pressures: an experimental study using aggregates of diamond. In: *Earth Processes: Reading the Isotopic Clock. Geophysical Monograph, American Geophysical Union* **95,** 109–122.

Langmuir, C. H., Klein, E. M. & Plank, T., 1992. Petrological systematics of mid-ocean ridge basalts: constraints on melt generation beneath ocean ridges. In: *Mantle Flow and Melt Generation at Mid-ocean Ridges. Geophysical Monograph, American Geophysical Union* **71,** 183–280.

Leake, B. E., 1978. Nomenclature of amphiboles. *American Mineralogist* **63,** 1023–1052.

Le Bas, M. J. & Streckeisen, A. L., 1991. The IUGS systematics of igneous rocks. *Journal of the Geological Society, London* **148,** 825–833.

Macdonald, R., McGarvie, D. W., Pinkerton, H., Smith, R. L. & Palacz, Z. A., 1990. Petrogenetic evolution of the Torfajøkull volcanic complex, Iceland I. Relationship between the magma types. *Journal of Petrology* **31,** 429–459.

Macdougall, J. D. & Lugmair, G. W., 1986. Sr and Nd isotopes in basalts from the East Pacific Rise: significance for mantle heterogeneity. *Earth and Planetary Science Letters* **77,** 273–284.

Mahoney, J. J., Sinton, J. M., Kurz, M. D., Macdougall, J. D., Spencer, K. J. & Lugmair, G. W., 1994. Isotope and trace element characteristics of a super-fast spreading ridge: East Pacific rise, 13–23°S. *Earth and Planetary Science Letters* **121,** 173–193.

Mammerickx, J., 1981. Depth anomalies in the Pacific: active, fossil and precursor. *Earth and Planetary Science Letters* **53,** 147–157.

McBirney, A. R. & Gass, I. G., 1967. Relations of oceanic volcanic rocks to mid-oceanic rises and heat flow. *Earth and Planetary Science Letters* **2,** 265–276.

Naar, D. F. & Hey, R. N., 1991. Tectonic evolution of the Easter Microplate. *Journal of Geophysical Research* **96,** 7961–7993.

Nielsen, R. L., 1990. Simulation of igneous differentiation processes. *Reviews in Mineralogy* **24,** 65–105.

O'Connor, J. M., Stoffers, P. & McWilliams, M. O., 1995. Time–space mapping of Easter Chain volcanism. *Earth and Planetary Science Letters* **136,** 197–212.

O'Nions, R. K. & Grönvold, K., 1973. Petrogenetic relationships of acid and basic rocks in Iceland: Sr-isotopes and rare-earth elements in late and postglacial volcanics. *Earth and Planetary Science Letters* **19,** 397–409.

O'Nions, R. K. & McKenzie, D. P., 1988. Melting and continent generation. *Earth and Planetary Science Letters* **90,** 449–456.

Oskarsson, N., Sigvaldason, G. E. & Steinthorsson, S., 1982. A dynamic model of rift zone petrogenesis and the regional petrology of Iceland. *Journal of Petrology* **23,** 28–74.

Parsons, B. & Sclater, J., 1977. An analysis of ocean floor bathymetry and heat flow with age. *Journal of Geophysical Research* **82,** 803–827.

Philpotts, J. A. & Schnetzler, C. C., 1970. Phenocryst–matrix partition coefficients for K, Rb, Sr and Ba, with applications to anorthosite and basalt genesis. *Geochimica et Cosmochimica Acta* **34,** 307–322.

Presnall, D. C., Dixon, J. R., O'Donnell, T. H. & Dixon, S. A., 1979. Generation of mid-ocean ridge tholeiites. *Journal of Petrology* **20,** 3–35.

Ribe, N. M. & Smooke, M. D., 1987. A stagnation point flow model for melt extraction from a mantle plume. *Journal of Geophysical Research* **92,** 6437–6443.

Roeder, P. L. & Emslie, R. F., 1970. Olivine–liquid equilibrium. *Contributions to Mineralogy and Petrology* **29,** 275–289.

Ryan, M. P., 1993. Neutral buoyancy and the structure of mid-ocean ridge magma reservoirs. *Journal of Geophysical Research* **93,** 22321–22338.

Schilling, J.-G., Sigurdsson, H., Davis, A. N. & Hey, R. N., 1985. Easter microplate evolution. *Nature* **317,** 325–331.

Searle, R. C., Bird, R. T., Rusby, R. I. & Naar, D. F., 1993. The development of two oceanic microplates: Easter and Juan Fernandez microplates, East Pacific Rise. *Journal of the Geological Society, London* **150,** 965–976.

Sinton, J. M. & Detrick, R. S., 1992. Mid-ocean ridge magma chambers. *Journal of Geophysical Research* **97,** 197–216.

Spengler, S. R. & Garcia, M. O., 1988. Geochemistry of the Hawi lavas, Kohala volcano, Hawaii. *Contributions to Mineralogy and Petrology* **99,** 90–104.

Stoffers, P., Hékinian, R., Haase, K. M. and the SO-80 Scientific Party, 1994. Geology of young submarine volcanoes west of Easter Island, Southeast Pacific. *Marine Geology* **118,** 177–185.

Stolper, E. & Walker, D., 1980. Melt density and the average composition of basalt. *Contributions to Mineralogy and Petrology* **74,** 7–12.

Sun, S.-s. & McDonough, W. F., 1989. Chemical and isotopic systematics of oceanic basalts: implications for mantle composition and processes. In: Saunders, A. D. & Norry, M. J. (eds) *Magmatism in the Ocean Basins. Geological Society of London Special Publication* **42,** 313–345.

Takahashi, E. & Kushiro, I., 1983. Melting of a dry peridotite at high pressures and basalt magma genesis. *American Mineralogist* **68,** 859–879.

Taylor, H. P., Jr, 1968. The oxygen isotope geochemistry of igneous rocks. *Contributions to Mineralogy and Petrology* **19,** 1–71.

Taylor, H. P., Jr & Sheppard, S. M. F., 1986. Igneous rocks: I. Processes of isotopic fractionation and isotope systematics. *Reviews of Mineralogy* **16,** 227–271.

White, W. M. & Hofmann, A. W., 1982. Sr and Nd isotope geochemistry of oceanic basalts and mantle evolution. *Nature* **296,** 821–825.

White, W. M., Hofmann, A. W. & Puchelt, H., 1987. Isotope geochemistry of Pacific mid-ocean ridge basalt. *Journal of Geophysical Research* **92,** 4881–4893.

Wilson, M., Downes, H. & Cebria, J.-M., 1995. Contrasting fractionation trends in coexisting continental alkaline magma series; Cantal, Massif Central, France. *Journal of Petrology* **36,** 1729–1753.

Woodhead, J. D. & McCulloch, M. T., 1989. Ancient seafloor signals in Pitcairn Island lavas and evidence for large amplitude, small length-scale mantle heterogeneities. *Earth and Planetary Science Letters* **94,** 257–293.

Woods, M. T. & Okal, E. A., 1994. The structure of the Nazca ridge and Sala y Gomez seamount chain from the dispersion of Rayleigh waves. *Geophysical Journal International* **117,** 205–222.

Yang, H.-J., Frey, F. A., Garcia, M. O. & Clague, D. A., 1994. Submarine lavas from Mauna Kea volcano, Hawaii: implications for Hawaiian shield stage processes. *Journal of Geophysical Research* **99,** 15577–15594.

Yang, H.-J., Frey, F. A., Rhodes, J. M. & Garcia, M. O., 1996. Evolution of Mauna Kea volcano: inferences from lava compositions recovered in the Hawaii Scientific Drilling Project. *Journal of Geophysical Research* **101,** 11747–11767.

Yoder, H. S. & Tilley, C. E., 1962. Origin of basalt magmas: an experimental study of natural and synthetic rock systems. *Journal of Petrology* **3,** 342–532.

Zindler, A., Staudigel, H. & Batiza, R., 1984. Isotope and trace element geochemistry of young Pacific seamounts: implications for the scale of upper mantle heterogeneity. *Earth and Planetary Science Letters* **70,** 175–195.